

Electrostatic Interactions in Strongly-Coupled Soft Matter

Ali Naji,^{1, 2,*} Swetlana Jungblut,² André G. Moreira,³ and Roland R. Netz^{4, 2}

¹*Physics Department, Technical University of Munich, James Franck St.,
D-85748 Garching, Germany.*

²*Physics Department, Ludwig Maximilian University, Theresienstr. 37,
D-80333 Munich, Germany.*

³*Polymer Physics, BASF Aktiengesellschaft, 67056 Ludwigshafen, Germany.*

⁴*Physics Department, Technical University Munich, James Franck Str.,
D-85748 Garching, Germany.*

Charged soft-matter systems—such as colloidal dispersions and charged polymers—are dominated by attractive forces between constituent like-charged particles when neutralizing counterions of high charge valency are introduced. Such counter-intuitive effects indicate strong electrostatic coupling between like-charged particles, which essentially results from electrostatic correlations among counterions residing near particle surfaces. In this paper, the attraction mechanism and the structure of counterionic correlations are discussed in the limit of strong coupling based on recent numerical and analytical investigations and for various geometries (planar, spherical and cylindrical) of charged objects.

PACS numbers: 82.70.-y; 87.15.-v; 61.20.Ja

Keywords: Electrostatic correlations; charged membranes, colloids and polymers; counterion condensation

I. INTRODUCTION

Electrostatic interactions and processes involving electric charges appear ubiquitously in biological and soft-matter systems. Electric charges make materials water-soluble and lead to many important technological and biological applications. In industry, for example, the stability of colloidal dispersions is often a desirable property as in the case of paints and food emulsions such as milk. One way to stabilize colloidal suspensions against coagulation or flocculation (occurring due to attractive van-der-Waals forces) is to generate long-range repulsive interactions between constituent colloidal particles by imparting permanent like-charges to these particles [1, 2, 3], or by grafting charged polymeric chains to their surfaces (forming hairy particles or polymeric brushes) [4]. Charged polymers, or the so-called *polyelectrolytes*, and their synthesis have also attracted a lot of attention [5] since, due to their water-solubility, they offer a useful option in design and processing of non-toxic environmentally-friendly materials. In biology, on the other hand, electrostatic effects emerge in many striking examples such as the DNA-packaging process in the cell nucleus. In each human cell, a total length of about 2m of DNA—which bears a total negative charge of about $10^{10}e$ (*i.e.* one elementary charge, e , per 1.7\AA)—is stored inside the cell nucleus with a diameter of less than $10\mu\text{m}$. This storage process involves a hierarchical structure on the lowest level of which, short segments of DNA are tightly wrapped around positively charged proteins of few-nanometer size (the so-called Histones). It is shown experimentally [6] that such a tightly wrapped state is only stable for intermediate, physiological salt concentrations, at which an optimal balance between self-repulsion of DNA segments and the DNA-Histone attraction is achieved.

Charged macromolecules (macroions) in solution are always surrounded by neutralizing counterions, and also in general by coions. Counterions form electrostatically-bound clouds in the proximity of macroions and in many cases, predominantly determine the electric properties of charged solutions [3]. In particular, counterions can alter the effective interaction between like-charged macroions, and may generate a dominant electrostatic attraction between them in certain physical conditions [7, 8, 9, 10, 11, 12, 13, 14, 15, 16, 17, 18, 19, 20, 21, 22, 23, 24, 25, 26, 27, 28, 29, 30, 31, 32, 33, 34, 35, 36, 37, 38, 39, 40, 41, 42, 43, 44, 45, 46, 47, 48, 49, 50, 51, 52, 53, 54, 55, 56, 57, 58, 59, 60, 61, 62, 63, 64, 65, 66, 67, 68, 69, 70, 71, 72, 73, 74, 75, 76, 77, 78]. Like-charge attraction manifests itself in a number of famous examples, namely, the condensation of DNA molecules [10], bundle formation of stiff polymers [16] and aggregation of colloidal particles [32, 33, 34]. Interestingly, such an attraction emerges only in *strongly-coupled* systems, *e.g.* when macroions are highly charged (with surface charge densities up to $1e/\text{nm}^2$ as in the DNA system), neutralizing counterions are multivalent, or when the temperature or the dielectric constant of medium is low. For instance, the

*Electronic address: naji@ph.tum.de

DNA condensation process, in which long DNA molecules condense into a tightly packed, circumferentially wound torus, is observed in experiments where multivalent counterions (such as trivalent spermidine ions) are introduced [10]. A similar trend has also been found in numerous numerical simulations of like-charged membranes, colloids and polymers [19, 20, 21, 22, 23, 24, 25, 26, 27, 28, 29, 30, 31, 32, 33, 34, 35, 36, 37, 38, 39, 40, 41, 42], where highly charged macroions are found to form closely-packed bound states due to attractive forces of electrostatic origin. These attractive forces are of typically large strength compared to the usual van-der-Waals attraction and may have significant practical implications where, for instance, multivalent counterions are present.

In the weak-coupling condition, *e.g.* when surface charge densities and charge valency of counterions are small, macroions are found to repel each other. In fact, from a theoretical point of view, one can argue that weakly-coupled systems should be described well by the mean-field approximation. Therefore, the effective interaction between macroions may be calculated using the mean-field solution for the electrostatic potential field in space, which follows from the so-called Poisson-Boltzmann (PB) equation that has been widely studied in the past [1, 2, 3]. It is known that the Poisson-Boltzmann theory—despite its success in many applications—can only yield repulsion between like-charged macroions [79, 80, 81].

The main scenarios which are put forward to explain the phenomenon of like-charge attraction have gone beyond the mean-field level by demonstrating that this phenomenon can be reproduced quantitatively by inclusion of electrostatic correlations [19, 20, 21, 22, 23, 24, 25, 26, 27, 28, 29, 30, 31, 32, 33, 34, 35, 36, 37, 38, 39, 40, 41, 42, 43, 44, 45, 46, 47, 48, 49, 50, 51, 52, 53, 54, 55, 56, 57, 58, 59, 60, 61, 62, 63, 64, 65, 66, 67, 68, 69, 70, 71, 72, 73, 74, 75, 76]. These correlations are systematically neglected on the mean-field level but become enhanced in strong-coupling conditions mentioned above. Recent theoretical attempts to incorporate ionic correlations include integral-equation methods [25, 43], perturbative improvement of the mean-field theory including Gaussian-fluctuations theories [44, 45, 46, 47, 48, 49, 50, 51, 52, 53, 54, 55, 56, 57], and local density functional theory [59, 60], which compare well with numerical simulations and all exhibit attraction. These methods are mostly applicable for large separations between macroions or in the regime of low coupling strengths (the so-called *high-temperature* regime), and can not characterize the closely-packed bound state between like-charged macroions. An alternative approach was triggered by Rouzina and Bloomfield [61] with the insight that counterions form two-dimensional highly-correlated layers at macroionic surfaces for high coupling strengths (the so-called *low-temperature* regime). Such structural correlations give rise to attractive forces [62, 63, 64, 65, 66, 67, 68, 69, 70, 71], which mainly result from energetic origins and can account for the closely-packed bound state of like-charged macroions [38, 39, 41, 62, 63, 64, 65, 66, 67, 68, 69, 70, 71].

In this paper, we shall chiefly consider this latter regime of strong coupling. First we shall briefly discuss the regime of parameters where electrostatic correlations are expected to be small or large in terms of the main length scales in a charged system (Section II). In Sections II-IV, we shall focus on the system of counterions at one or two planar charged walls to demonstrate the gross physical picture in both weak-coupling (or mean-field) and strong-coupling regimes. The role of curvature and its main physical consequences are considered in Sections VI-VIII. As we shall see, the so-called counterion-condensation process occurring at curved surfaces plays an important role in determining the attraction regime between spherical (Section VII) and cylindrical (Section VIII) macroions. We focus on analytical results only based on two exact asymptotic theories, namely, the mean-field Poisson-Boltzmann theory and the strong-coupling (SC) theory. The crossover regime between these two limits are considered using recent numerical simulations, which are useful to determine the regime of applicability of both asymptotic theories, and also to examine the validity of their predictions.

We restrict our discussion to a primitive model in which particles only interact with Coulombic forces and in some cases, also with short-range excluded-volume repulsions. The inhomogeneous charge distribution of macroions and also ion-surface adsorption effects [77] are neglected. We do not consider coions and take the solvent effects into account only through the continuum dielectric constant of medium ϵ (for water at room temperature $\epsilon \approx 80$), which is mainly assumed to be uniform and equal everywhere in space. The role of the dielectric jump at charged boundaries will be discussed briefly in Section V for the case of two charged walls.

II. LENGTH SCALES IN CHARGED SYSTEMS: FROM MEAN-FIELD TO STRONG-COUPLING REGIME

To distinguish the regimes of parameters where attractive or repulsive forces may arise between macroions, one needs first to study the length scales that appear in a classical charged system. Let us consider a system of macroions with uniform surface charge density of $-\sigma_s$ (in units of the elementary charge e) and neutralizing counterions of charge valency q at temperature T . (Hereafter, we conventionally assume that macroions are negatively charged and counterions are positively charged, thus σ_s and q are both positive by definition.)

A characteristic length scale in such a system is set by comparing the thermal energy scale, $k_B T$, with the Coulombic interaction energy between counterions, $V(r) = q^2 e^2 / (4\pi \epsilon \epsilon_0 r)$, where r is the distance between two given counterions.

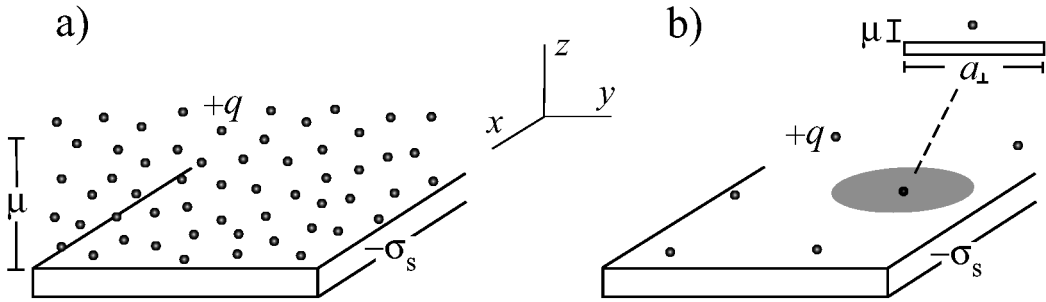


FIG. 1: a) For small coupling parameter, $\Xi \ll 1$, counterions form a diffuse three-dimensional layer. b) For large coupling parameter, $\Xi \gg 1$, the counterionic layer is essentially two dimensional since the typical lateral distance between counterions, a_{\perp} , becomes much larger than the Gouy-Chapman length, μ . In this regime, counterions are strongly correlated and surrounded by a correlation hole of size $\sim a_{\perp} \gg \mu$.

The ratio between these two quantities may be written as $V/(k_B T) = q^2 \ell_B / r$, where

$$\ell_B = \frac{e^2}{4\pi\epsilon_0 k_B T} \quad (1)$$

is the so-called Bjerrum length, which measures the distance at which two elementary charges interact with thermal energy $k_B T$ (in water and at room temperature $\ell_B \approx 7 \text{ \AA}$). Thus the rescaled Bjerrum length

$$\tilde{\ell}_B = q^2 \ell_B \quad (2)$$

may be taken as the relevant length scale to characterize the strength of mutual counterionic repulsions against thermal fluctuations in the system.

Other length scales are set by considering the charge distribution and the specific geometry of macroions. For simplicity, let us concentrate here on a *planar* system composed of a planar charged wall of infinitely-large extension and neutralizing counterions confined to one half-space (Figure 1). This model is physically relevant for charged membranes and also for macroions with large radii of curvature, which behave like plates at small distances from their surface.

In this system, an additional length scale may be obtained by comparing the thermal energy $k_B T$ with the energy scale of the counterion-wall attraction, $U(z) = q\sigma_s e^2 z / (2\epsilon\epsilon_0)$, where z is the vertical distance from the wall. Hence we have the ratio $U/(k_B T) = z/\mu$, where

$$\mu = \frac{1}{2\pi q \ell_B \sigma_s} \quad (3)$$

gives the so-called Gouy-Chapman length, which measures the distance at which the thermal energy equals the counterion-wall interaction energy. The Gouy-Chapman length also gives a measure of the thickness of the counterionic layer at a charged wall, $\langle z \rangle \sim \mu$, as we shall see later.

In principle, one may tune the system parameters in such a way that either of the two length scales $\tilde{\ell}_B$ and μ become arbitrarily large or small. In fact, only the dimensionless ratio between these two quantities is relevant and uniquely describes the physical regimes of the system [82], namely,

$$\Xi = \frac{\tilde{\ell}_B}{\mu} = 2\pi q^3 \ell_B^2 \sigma_s, \quad (4)$$

which is known as the *electrostatic coupling parameter*. For small coupling parameter $\Xi \ll 1$, the counterion-wall system has a relatively large Gouy-Chapman length (or small Bjerrum length), which indicates a loosely bound counterion cloud at the charged wall (Figure 1a). For large coupling parameter $\Xi \gg 1$, the Gouy-Chapman length is relatively small (or the Bjerrum length is large) indicating that counterions are strongly attracted toward the charged wall (Figure 1b).

Further insight into the structure of the counterionic layer may be obtained by considering the typical distance between counterions at the surface. For counterions residing near the charged surface, the local electroneutrality condition implies a typical lateral separation of

$$a_{\perp} \sim \sqrt{\frac{q}{\sigma_s}}, \quad (5)$$

Charged object	σ_s (e/nm ²)	R (Å)	q	μ (Å)	Ξ	ξ
charged membranes	~ 1	—	1	2.2	3.1	—
			2	1.1	24.8	—
			3	0.7	83.7	—
DNA	0.9	10	1 (Na ⁺)	2.4	2.8	4.1
			2 (Mn ²⁺)	1.2	22.4	8.2
			3 (spermidine)	0.8	75.6	12.3
			4 (spermine)	0.6	179	16.4
highly charged colloids (surfactant micelles)	~ 1	20	3	0.7	85	28
weakly charged colloids (polystyrene particles)	~ 0.1	$\sim 10^3$	1	~ 2	~ 0.1	$\sim 5 \times 10^2$

TABLE I: Typical values of physical parameters for realistic charged systems: σ_s and R denote the surface charge density and the radius of curvature of charged objects, q is the charge valency of counterions, and μ , Ξ and ξ are the Gouy-Chapman length, $\mu = 1/(2\pi q\ell_B \sigma_s)$ (Eq. (3)), the coupling parameter, $\Xi = q^2 \ell_B / \mu$ (Eq. (4)), and the Manning parameter, $\xi = R/\mu$ (Eq. (26)), respectively. (The role of curvature and Manning parameter for cylindrical and spherical macroions is discussed in Sections VI-VIII.) The Bjerrum length is taken here as $\ell_B \approx 7.1$ Å corresponding to an aqueous medium of dielectric constant $\epsilon = 80$ at room temperature.

since each counterion neutralizes the charge of an area given by $a_\perp^2 \sim q/\sigma_s$ (up to a geometrical prefactor of the order one). Comparing this length scale with the Gouy-Chapman length, we have

$$\frac{a_\perp}{\mu} \sim \sqrt{\Xi}. \quad (6)$$

Hence in the strong-coupling regime, $\Xi \gg 1$, counterions essentially form a quasi two-dimensional layer as their lateral separation at surface becomes much larger than the Gouy-Chapman length $a_\perp \gg \mu$ (Figure 1b). On the other hand, the structure of such a layer is dominated by mutual repulsions between counterions, which freeze out lateral degrees of freedom. Hence counterions become laterally correlated and surrounded by a large *correlation hole* of size a_\perp from which neighboring counterions are statistically depleted [61, 64, 66] (see Section III C for a more detailed analysis [39]). This indicates a trend toward crystallization in the ionic structure for increasing coupling parameter, which can be corroborated by considering the effective plasma parameter relevant for this situation

$$\Gamma = \frac{\tilde{\ell}_B}{a_\perp} \sim \Xi^{1/2}. \quad (7)$$

The parameter Γ gives a measure of mutual Coulombic repulsions between counterions at a neutralizing surface (the 2D one-component plasma) [61, 64, 66]. For increasing Ξ , Γ increases while the average counterion-wall interaction (per $k_B T$) remains of the order of unity, $\langle U \rangle / (k_B T) = \langle z \rangle / \mu \sim 1$. The Wigner crystallization of the 2D one-component plasma is known to occur for $\Gamma > \Gamma_c \approx 125$ [83], which corresponds to the range of coupling parameters $\Xi > \Xi_c \approx 3.1 \times 10^4$ [39] (see Section III C).

In the weak-coupling regime ($\Xi \ll 1$), no crystallization is expected to occur and the counterion layer has a three-dimensional fluid-like structure ($a_\perp \ll \mu$) [84] (Figure 1a). Thus the two asymptotic regimes of weak coupling ($\Xi \ll 1$) and strong coupling ($\Xi \gg 1$) may be distinguished physically by the structure of counterionic layers at charged surfaces. In Sections III and IV, we shall briefly review the main results obtained in each of these regimes for the classical example of counterions at one and two charged walls (planar double layers).

But before proceeding further, it is useful to consider the typical values of the coupling parameter in realistic systems. In Table I, we show few typical examples of both weakly-coupled and strongly-coupled systems. As already seen from Eq. (4), the coupling strength grows quite rapidly with the counterion valency ($\Xi \sim q^3$), which agrees with experimental and numerical evidence indicating highly growing correlation effects for increasing counterion valency [7, 8, 9, 10, 11, 12, 13, 14, 15, 16, 17, 18, 19, 20, 21, 22, 23, 24, 25, 26, 27, 28, 29, 30, 31, 32, 33, 34, 35, 36, 37, 38, 39, 40, 41, 42]. In fact as known from these studies, typical coupling strength of $\Xi \sim 10^2$ (or larger) already reflects strong-coupling regime and a value of $\Xi \sim 1$ (or smaller) typically corresponds to the weak-coupling regime.

III. COUNTERIONS AT A CHARGED WALL

A. Weak-coupling (or Mean-field) regime $\Xi \ll 1$

For small coupling strength, one may employ the mean-field approximation to describe the counterionic layer since each counterion interacts with a diffuse cloud of other counterions. The mean-field approximation systematically neglects correlations among counterions and is formally valid in the strict limit of $\Xi \rightarrow 0$ [55].

The mean-field theory is governed by the so-called Poisson-Boltzmann (PB) equation [1, 2, 55]

$$\nabla^2 \psi(\mathbf{x}) = -\frac{qe\rho_0}{\varepsilon\varepsilon_0} \exp(-qe\psi/k_B T), \quad (8)$$

which is to be solved for the mean electrostatic potential in space, ψ , using proper boundary conditions at macroion surfaces. The corresponding density profile of counterions, $\rho_{\text{PB}}(\mathbf{x})$, follows from the solution of the PB equation (8) and using the relation $\rho_{\text{PB}}(\mathbf{x}) = \rho_0 \exp(-qe\psi/k_B T)$, where ρ_0 is a normalization prefactor.

For the system of point-like counterions at a single uniformly-charged wall (in the absence of salt), the PB theory predicts an algebraically-decaying density profile of the form [1, 2]

$$\frac{\rho_{\text{PB}}(z)}{2\pi\ell_B\sigma_s^2} = \frac{1}{(z/\mu + 1)^2}, \quad (9)$$

where z is the distance from the wall. The density of counterions at contact is obtained as $\rho(z=0) = 2\pi\ell_B\sigma_s^2$, which is an exact result within the present model and valid beyond the mean-field level [85]. As seen the PB theory predicts an extended counterionic density profile (with diverging moments) in agreement with the qualitative considerations in Section II for a weakly-coupled system. Nonetheless, the PB density profile (9) is normalizable to the total number of counterions reflecting the fact a charged wall binds all its counterions. Note also that the Gouy-Chapman length, μ , in this case equals the height of a layer at the wall which contains half of the counterions, and thus may be associated with the typical layer thickness at low couplings.

B. Strong-coupling regime $\Xi \gg 1$

In this regime, the liquid-like ordering (or crystallization at sufficiently large couplings) of counterions renders the mean-field theory an invalid description of the system. Yet one can obtain a simple analytical description for the counterionic layer as follows [61, 64, 66, 69].

Since for $\Xi \gg 1$ counterions become highly separated from each other in a quasi-2D layer at the charged wall (Figure 1b), one may consider the system as a collection of laterally frozen *correlation cells*, each consisting of a single counterion interacting with an area of the wall of size $\sim a_{\perp}$ (Eq. (5)). Since in this regime $a_{\perp} \gg \mu$, the dominant contribution to the density profile of counterions at the wall is obtained by considering only the vertical degree of freedom, z , through which single counterions are coupled to the wall with the interaction potential $U/(k_B T) \approx z/\mu$. Hence using the Boltzmann weight, one has the following density profile

$$\rho_{\text{SC}}(z) = \rho_0 \exp(-z/\mu). \quad (10)$$

The prefactor in the above expression (the contact density) may be fixed from the normalization condition for the density profile and the global electroneutrality of the system as $\rho_0 = 2\pi\ell_B\sigma_s^2$. The strong-coupling density, $\rho_{\text{SC}}(z)$, drops quite rapidly as one moves away from the charged wall. The average distance of counterions is obtained to be equal to the Gouy-Chapman length, $\langle z \rangle_{\text{SC}} = \mu$.

The above density profile, which essentially follows from single-particle contributions, was obtained by Shklovskii [64, 66] using a Wigner-crystal model for large Coulombic coupling. The asymptotic analysis of Ref. [69] showed that the partition function of the system for $\Xi \rightarrow \infty$ adopts a series expansion in powers of $1/\Xi$, the leading term of which is given only by single-particle contributions. The multi-particle contributions enter in higher-order terms (in the form of a virial expansion). The leading term defines the *asymptotic* strong-coupling (SC) theory, which for the counterion-wall system gives exactly the density profile (10).

C. Intermediate-coupling regime

In realistic systems, the coupling parameter is always finite (see Table I). Therefore, it is important to examine whether and how the preceding analytical results for the two limits of strong ($\Xi \rightarrow \infty$) and weak ($\Xi \rightarrow 0$) coupling

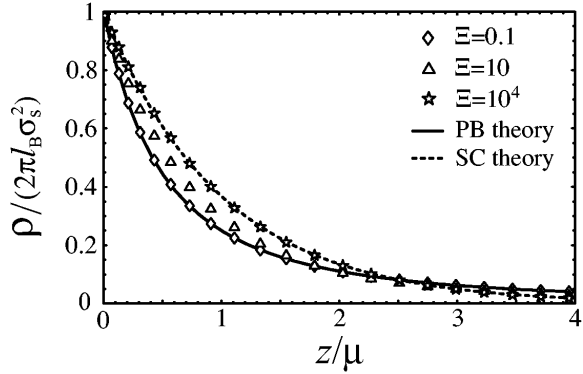


FIG. 2: Density profile of counterions at a charged wall as a function of the distance from the wall, z . The symbols are the data from Monte-Carlo simulations for $\Xi = 0.1$ (open diamonds), $\Xi = 10$ (open triangles) and $\Xi = 10^4$ (open stars). The solid curve and the dashed curve represent the predictions of the mean-field (PB) theory, Eq. (9), and the strong-coupling theory, Eq. (10), respectively. The density profile is rescaled by its values at contact $\rho(z = 0) = 2\pi\ell_B\sigma_s^2$ and the distance from the wall is shown in units of the Gouy-Chapman length, μ .

may be applied to such systems. A useful approach to investigate the regime of intermediate couplings is to employ numerical simulation methods. Other methods include systematic improvement of both mean-field and strong-coupling theories [69] that will be considered only for the interaction between two walls in Section IV.

The density profile of counterions at an infinitely large charged wall has been calculated for various coupling parameters using Monte-Carlo simulations in Ref. [37]. (The simulation model is similar to what we described in Section II (Figure 1), where counterions are taken as point-like particles confined to one half-space and periodic boundary conditions are used in lateral directions [39].) In Figure 2, we show the simulated density profile of counterions (symbols) for coupling parameters $\Xi = 0.1, 10$ and 10^4 along with the analytical predictions of the mean-field PB theory (solid curve, Eq. (9)) and the strong-coupling theory (dashed curve, Eq. (10)). Note that in the Figure the distance from the wall is rescaled with the Gouy-Chapman length; hence, the PB and SC profiles appear to have a similar decay length of about unity in rescaled units. As seen, the data crossover from the mean-field (PB) prediction to the SC result by increasing Ξ , quantitatively confirming the validity of both theories at small couplings (about $\Xi = 0.1$) and large couplings (about $\Xi = 10^4$) respectively.

Further analysis of the simulated density profile [39] reveals a distance-dependent crossover at intermediate coupling parameters: while the large distance behavior of the system is described well by the mean-field theory, at sufficiently small distances from the wall, the system roughly follows the strong-coupling prediction at intermediate Ξ . This is in fact a quite general property that we shall investigate in more detail for the interaction between two charged walls in Section IV. The crossover in the single-wall system can be understood qualitatively by noting that the asymptotic strong-coupling density profile, Eq. (10), remains valid only within distances smaller than the correlation hole size $z < a_\perp$ [39, 64, 69, 86]. Thus at *finite* coupling parameters, the strong-coupling regime may be characterized by

$$\frac{z}{\mu} < \Xi^{1/2}, \quad (11)$$

where we have used Eq. (5). For distances, z , from the wall which are larger than a_\perp , lateral interactions between counterions become relevant and modify the density profile. For $z \gg a_\perp$, one intuitively expect that dominant many-body effects lead to a mean-field-like behavior as shown in previous studies [39, 69]. In fact, the mean-field results turn out to be valid for distances $z/\mu > \Xi$ (up to some logarithmic corrections) [39, 69].

An interesting problem is to examine the development of correlations between counterions (including the formation and size of the correlation hole) as the coupling parameter increases. This goal may be achieved by considering the two-dimensional pair distribution function of counterions, which is defined through

$$g_{2D} = \frac{A}{N^2} \left\langle \sum_{\langle ij \rangle} \delta(\mathbf{r}_{xy} - \mathbf{r}_{xy,i} + \mathbf{r}_{xy,j}) \right\rangle, \quad (12)$$

where the sum runs over pairs of particles, \mathbf{r}_{xy} is a 2D vector and $\mathbf{r}_{xy,i}$ is the lateral position of particle i in the xy -plane (see Figure 1). Physically g_{2D} gives the ratio between the probability of finding two counterions at distance $r_{xy} = |\mathbf{r}_{xy}|$ from each other and the expected probability for a homogeneous 2D fluid with the same bulk density.

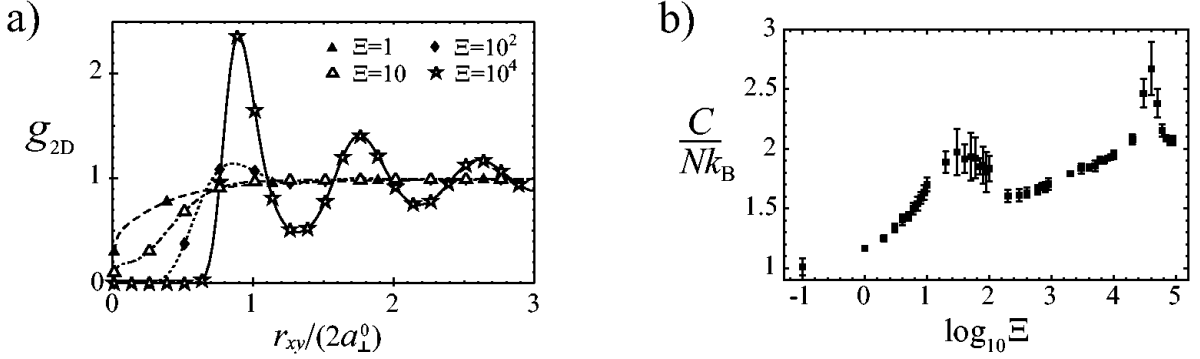


FIG. 3: a) The two-dimensional pair distribution function of counterions at a charged planar wall plotted as a function of the lateral distance between counterions (the distribution function is obtained by averaging over the height z). The symbols are the data from Monte-Carlo simulations for $\Xi = 1$ (filled triangles), $\Xi = 10$ (open triangles), $\Xi = 100$ (filled diamonds) and $\Xi = 10^4$ (open stars). The lateral distance is rescaled by the length scale $2a_1^0 = 2\sqrt{q/(\pi\sigma_s)}$, which gives a measure of lateral separation between counterions (see the text).

b) The simulated excess heat capacity of the system of counterions at a charged wall (per number of counterions, N) plotted as a function of the coupling parameter, Ξ . (The number of counterions in this case is $N = 100$ in a square simulation box, which is periodically replicated in lateral directions.) The broad hump at intermediate couplings ($10 < \Xi < 100$) reflects the structural change in the counterionic layer due to increasing correlations between counterions. At large coupling strength ($\Xi \approx 3.1 \times 10^4$), the counterionic layer undergoes a crystallization process indicated by a pronounced peak in the heat capacity.

The Monte-Carlo results for this quantity are shown in Figure 3a [39]. It shows that for small coupling parameter ($\Xi = 1$, filled triangles), there is only a very short-range depletion zone at small separations between counterions. But a pronounced correlation hole is created at the regime of coupling parameters $10 < \Xi < 100$, where the distribution function vanishes over a finite range at small inter-particle separations. For larger coupling strengths, the correlation hole becomes more pronounced and is followed by an oscillatory behavior in the pair distribution function ($\Xi = 10^4$, open stars). This indicates a liquid-like order in the counterionic structure in agreement with qualitative considerations in Section II. Note that the distance coordinate in Figure 3a is rescaled with $2a_1^0$, where $a_1^0 = \sqrt{q/(\pi\sigma_s)}$ is obtained by assuming that the area of the wall neutralized by a counterion has a circular form (Figure 1b). The location of the first peak of g_{2D} for $\Xi = 10^4$ appears at a distance of $r_{xy}/(2a_1^0) \approx 0.9$, which roughly gives the typical lateral distance between counterions. In a perfect hexagonal crystal, the peak is expected to occur at $r_{xy}/(2a_1^0) = \sqrt{\pi/(2\sqrt{3})} \approx 0.95$, and in a perfect square crystal at $r_{xy}/(2a_1^0) = \sqrt{\pi}/2 \approx 0.89$. The crystallization is in fact found at even larger coupling parameters [87], which may be seen also from the behavior of the heat capacity for increasing Ξ .

In Figure 3b, the simulated excess heat capacity of the counterion-wall system (obtained by omitting the trivial kinetic energy contribution $3k_B/2$) is shown for various coupling parameters. The crystallization of counterions at the wall is reflected by a pronounced peak at large coupling parameters about $\Xi_c \approx 31000$, which roughly agrees with the Wigner-crystallization threshold of a 2D one-component plasma [83]. The characteristic properties of the crystallization transition in the counterion-wall system are yet to be specified, which requires a detailed finite-size scaling analysis in the vicinity of the transition point. Another interesting behavior is observed in Figure 3b at the range of coupling parameters $10 < \Xi < 100$, where the heat capacity exhibits a broad hump. This hump does not represent a phase transition [39], but it is associated with the onset of the correlation hole around counterions and the structural change in the counterionic layer from being a three-dimensional layer at low couplings to a quasi-2D layer at large couplings. In the region between the hump and the crystallization peak (for $200 < \Xi < 10^4$), the heat capacity is found to increase almost logarithmically with Ξ . The reason for this behavior is at present not clear.

IV. REPULSIVE AND ATTRACTIVE LIKE-CHARGE INTERACTIONS: PLANAR GEOMETRY

Now let us consider the interaction between macroions in the two regimes of mean field and strong coupling. In this Section, we focus on the the planar system of two parallel charged walls of uniform surface charge density $-\sigma_s$ at separation Δ from each, where q -valent counterions fill only the space between the walls (the dielectric constant is also assumed to be uniform in space)—see Figure 4. This model is relevant for interaction between two charged membranes or two macroions of large radii of curvature.

In this system, an extra length scale is set by the wall separation, Δ . Two limiting regimes of repulsion and

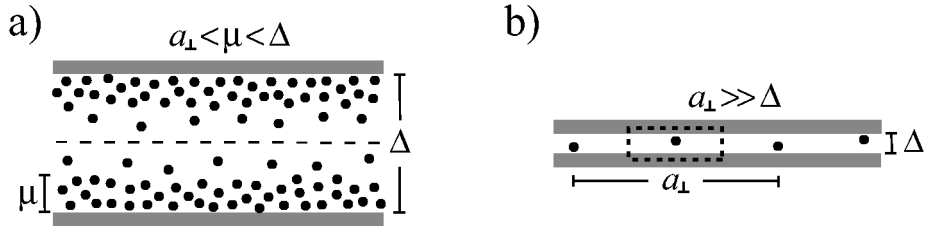


FIG. 4: Schematic representation of the asymptotic interaction regimes of a) mean field and b) strong coupling for two like-charged walls. The mean-field regime is obtained at large separations between the walls (compared to other length scales) and is dominated by the repulsive osmotic pressure of counterions. For small wall separation (compared with the typical counterion spacing), the walls attract each other since counterions are isolated in correlation cells of large lateral extension $\sim a_{\perp}/2 \gg \Delta$ (shown by a dotted loop) and mediate a dominant single-particle attraction between the walls.

attraction may be distinguished qualitatively by comparing Δ with other length scales of the system as follows.

A. Mean-field regime: repulsion

First consider the limit where the wall separation, Δ , is *large* compared with all other length scales in the system and also that the system is weakly coupled, $\Xi \ll 1$ (see Figure 4a). In this case, counterions form a diffuse layer at each wall, but due to large wall separation, the system is approximately decoupled into two nearly neutral sub-systems, each consisting of a charged wall and its counterionic cloud. The effective pressure acting between the walls is dominated by the osmotic pressure of counterions across the mid-plane, since the overall electrostatic field at the mid-plane is zero due to the charge neutrality of each sub-system. This osmotic pressure is positive and therefore gives an effective *repulsion* between the walls.

The mid-plane osmotic pressure is proportional to the local density of counterions, ρ_{mid} , following the ideal-gas equation $P = \rho_{\text{mid}} k_B T$, where ρ_{mid} drops roughly with the inverse square of the wall separation for large Δ as it follows from Eq. (9). This yields the scaling form of the repulsive pressure between the walls as $P(\Delta) \sim \Delta^{-2}$. The formal derivation of the pressure based on the PB equation supports the above result for large separation. The full PB solution for arbitrary Δ follows as [1, 2, 69]

$$\frac{\beta P_{\text{PB}}(\Delta)}{2\pi\ell_B\sigma_s^2} = \Lambda \quad (13)$$

(with $\beta = 1/k_B T$), where Λ is determined from the transcendental equation $\Lambda^{1/2} \tan[\Lambda^{1/2}(\Delta/2\mu)] = 1$. For large $\Delta/\mu \gg 1$, the PB solution yields

$$\frac{\beta P_{\text{PB}}(\Delta)}{2\pi\ell_B\sigma_s^2} \approx \left(\frac{\pi\mu}{\Delta}\right)^2, \quad (14)$$

which is expectedly independent of the surface charge density of the walls.

B. Strong-coupling regime: attraction

Now we consider a different asymptotic regime in which the system is strongly coupled, $\Xi \gg 1$, and the distance between the walls is smaller than the lateral spacing between counterions at each wall $a_{\perp} \gg \Delta$ (Figure 4b). Since counterions are highly separated from each other, the two opposite layers of counterions tend to form an inter-locking pattern at equilibrium, where each counterion from one layer faces a bare area of the other wall with nearly equal (but opposite) charge. It is evident that this pattern leads to an effective *attractive* force between the walls with a purely energetic origin. The effective pressure acting between the walls may be estimated using a simple argument that takes into account the highly correlated structure of counterions [61, 69].

In the asymptotic limit considered here (*i.e.* for $\Xi \gg 1$ and $a_{\perp} \gg \Delta$), each counterion is essentially confined and isolated in a “correlation cell” that consists of a single counterion sandwiched between two opposing sections of the walls with lateral size of about $a_{\perp}/2$ (Figure 4b). Since $a_{\perp} \gg \Delta$, the effective pressure between the walls is dominated by the contribution coming from each single correlation cell and lateral interactions between these cells may be neglected.

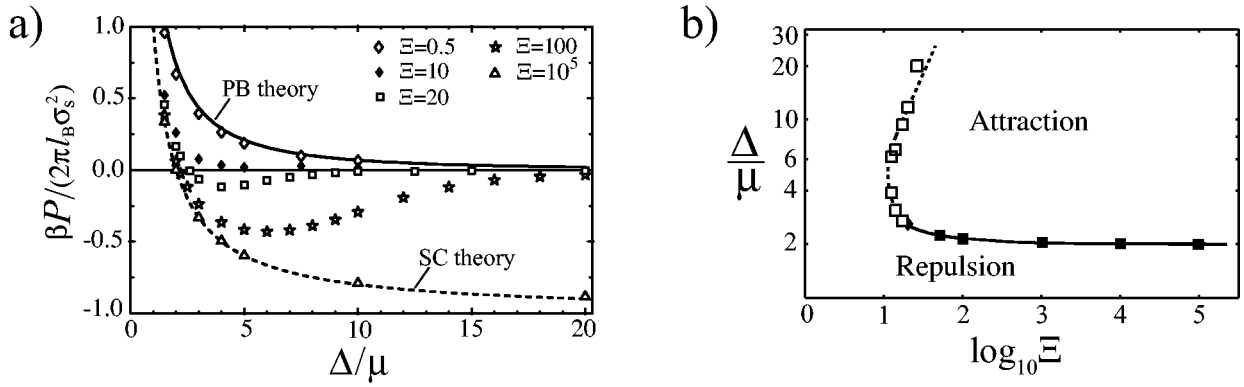


FIG. 5: a) Effective pressure between two like-charged walls as a function of their distance, Δ . The symbols are MC simulation data for $\Xi = 0.5$ (open diamonds), $\Xi = 10$ (filled diamonds), $\Xi = 20$ (open squares), $\Xi = 100$ (open stars) and $\Xi = 10^5$ (open triangles). The solid curve is the prediction of the mean-field PB theory, Eq. (13), and the dashed curve is the strong-coupling prediction, Eq. (15). The pressure and the wall separation are shown in rescaled units as indicated on the graph. b) Attraction and repulsion regimes shown in terms of the rescaled wall distance, Δ/μ , and the coupling parameter, Ξ . Symbols are the simulation results indicating the zero-pressure points (connecting lines are guides to the eye). Filled symbols show the thermodynamically stable bound state of the two walls at small separations. Open symbols indicate the meta-stable or unstable states of zero pressure. Attraction sets in for $\Xi > 12$ and a first-order phase transition occurs at $\Xi \approx 17$.

The electrostatic energy of the system per cell is the sum of the interactions between the two surfaces with each other and with the single counterion, which—using the electroneutrality condition and the fact that the wall separation is small—follows as $\beta u_e \approx 2\pi\ell_B\sigma_s^2\Delta$ per unit area. This *energetic* contribution gives an attractive pressure of $\beta P_e \approx -2\pi\ell_B\sigma_s^2$ between the walls. On the other hand, the entropic contribution due to the counterion confinement is of the order $S \sim k_B \ln \Delta$ (per cell), which generates a repulsive component. The total pressure between the walls is then obtained by combining these two effects and may be written as

$$\frac{\beta P_{SC}(\Delta)}{2\pi\ell_B\sigma_s^2} = -1 + \frac{2\mu}{\Delta}. \quad (15)$$

This expression clearly predicts a closely-packed *bound state* between the walls with equilibrium surface separation, Δ_* , being equal to twice the Gouy-Chapman length, *i.e.*

$$\Delta_* = 2\mu. \quad (16)$$

The like-charged walls attract each other for $\Delta > \Delta_*$ and repel at smaller distances.

The energetic attraction in the strong-coupling regime, which results from structural correlations, was first obtained by Rouzina and Bloomfield [61] and investigated later by several workers [62, 63, 64, 65, 66, 67, 68, 69, 70, 71]. The rigorous derivation of the expression (15) for the pressure was given using the asymptotic strong-coupling theory [69], which shows that Eq. (15) is the exact result in the limit of $\Xi \rightarrow \infty$.

Note that in the presence of counterions of finite diameter σ_{ci} , the equilibrium separation between the walls, Eq. (16), increases by an amount equal to the counterion diameter and reads

$$\Delta_* = \sigma_{ci} + 2\mu \quad (17)$$

assuming that counterions interact with a hard-core excluded-volume interaction with the walls. Clearly, the excluded-volume interaction between counterions themselves is irrelevant in the strong-coupling regime since counterions are highly separated from each other ($a_\perp \gg \Delta$).

C. Numerical simulations and the crossover regime

In order to examine the preceding asymptotic results in the mean-field and strong-coupling regimes, we consider the Monte-Carlo simulations of the two-wall system, which enable one to investigate the mechanism of like-charge interaction beyond the above limiting cases.

Figure 5a shows the simulated effective pressure acting between two like-charged walls (in the presence of point-like counterions) for various coupling parameters [38, 39]. The pressure becomes negative, and thus indicates attraction

between the walls at small and intermediate separations, when the coupling parameter exceeds an intermediate threshold (see below). The onset of attraction at intermediate couplings ($10 < \Xi < 100$) agrees with the onset of correlations between counterions as discussed in Section III C. For small couplings ($\Xi = 0.5$, open diamonds), the data quantitatively support the mean-field PB prediction (solid curve), Eq. (13), and for very large couplings ($\Xi = 10^5$, open triangles), they agree with the SC prediction (dashed curve), Eq. (15), quite well.

The behavior of the pressure may be summarized in a phase diagram as shown in Figure 5b, which shows the regions of positive (repulsive) and negative (attractive) pressure separated by a line of zero pressure. The attractive region only appears for coupling parameters $\Xi > 12$. The filled symbols (connected with a solid line) show the stable bound state of the two walls, while the open symbols (connected with a dashed line) correspond to meta-stable or unstable states of the two wall (*i.e.* the local minima or the maximum of the free energy of the system, where the free energy is obtained from the data by integrating the pressure from infinite distance to a finite distance, Δ) [39]. As seen, the stable bound state exhibits an equilibrium wall separation quite close to the strong-coupling prediction, $\Delta_*/\mu = 2$ (Eq. (16)), for moderate to large coupling parameters. The thermodynamic behavior of this system has been studied in Ref. [39], which predicts a first-order unbinding transition at $\Xi \approx 17$.

The effective pressure also exhibits a distance-dependent crossover at intermediate couplings [38, 39, 69]: at small wall separations, the data closely follow the SC curve, while for large separations, they tend to the PB curve and display a mean-field-like repulsion. In order to study the crossover behavior analytically, one needs to consider the extension of both asymptotic theories of mean field ($\Xi \rightarrow 0$) and strong coupling ($\Xi \rightarrow \infty$) to finite-coupling situations.

1. loop expansion: sub-leading corrections to the mean-field PB theory

The mean-field PB theory is obtained from a saddle-point approximation in the limit of $\Xi \rightarrow 0$ [55]. Therefore, one way to incorporate finite-coupling effects on a systematic level is to calculate the higher-order corrections to the saddle-point solution by means of a loop expansion. The loop parameter turns out to be the coupling parameter Ξ and the effective pressure between the walls may be expanded about the mean-field solution as

$$P(\Delta) = P_{\text{PB}}(\Delta) + \Xi P_{\text{PB}}^{(1)}(\Delta) + \mathcal{O}(\Xi^2), \quad (18)$$

where P_{PB} is the PB solution (13), and $P_{\text{PB}}^{(1)}$ is the first-loop or the Gaussian correction term [47, 48]

$$\frac{\beta P_{\text{PB}}^{(1)}}{2\pi\ell_B\sigma_s^2} \approx -\left(\frac{\mu}{\Delta}\right)^3 \left[\frac{\zeta(3)}{4} + \frac{\pi^3}{4} + \pi^2 \ln(\Delta/\mu) \right]. \quad (19)$$

Clearly, the Gaussian correction term contributes an attractive component, which comes from correlations between fluctuations in the counterionic clouds at opposite walls. These fluctuations tend to polarize each other giving rise to attraction in the same way as other fluctuation-induced attractive forces (such as dispersion interactions) are generated [54]. It is tempting to argue that the Gaussian correction term turns the net pressure between the walls into an attractive pressure for large enough Ξ . However, the onset of attraction in fact signals the break-down of the loop-expansion scheme as used above, since the correction term becomes comparable to the leading PB term [69]. Therefore, the Gaussian-fluctuations picture remains valid only at sufficiently small couplings (or the so-called *high-temperature regime*) and also for sufficiently large separations $\Delta/\mu \gg 1$ (see the discussion in Refs. [56, 68, 69]).

The regime of validity of the loop expansion (and that of the mean-field PB theory) at a *finite* coupling parameter, Ξ , may be estimated by comparing the sub-leading and the leading terms in Eq. (18), that gives [39, 69]

$$\frac{\Delta/\mu}{\ln(\Delta/\mu)} > \Xi. \quad (20)$$

2. virial expansion: sub-leading corrections to the strong-coupling theory

In the strong-coupling regime, the finite-coupling corrections may be taken into account using a virial-expansion scheme, which is obtained as a series expansion in powers of $1/\Xi$ about the asymptotic strong-coupling solution (for $\Xi \rightarrow \infty$) [69]. The effective pressure between two like-charged walls adopts the following large coupling expansion

$$P(\Delta) = P_{\text{SC}}(\Delta) + \frac{1}{\Xi} P_{\text{SC}}^{(1)}(\Delta) + \mathcal{O}(\Xi^{-2}), \quad (21)$$

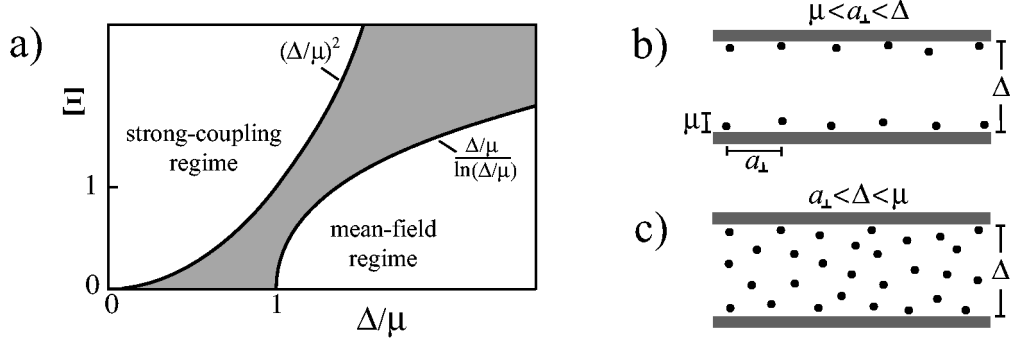


FIG. 6: a) Regimes of applicability of the asymptotic theories of mean field Poisson-Boltzmann and strong coupling for the system of two like-charged walls and counterions. There is an intermediate regime of rescaled distances between the walls, Δ/μ , and coupling parameters, Ξ , where finite-coupling effects can not be captured by series expansions around the mean-field or the strong-coupling solutions. Possible physical situations in this regime are schematically shown in b) and c)—see the text.

where P_{SC} is the SC prediction, Eq. (15), and $P_{\text{SC}}^{(1)}$ is the first correction term [38, 39, 69]

$$\frac{\beta P_{\text{SC}}^{(1)}}{2\pi\ell_B\sigma_s^2} = \frac{\Delta}{3\mu}, \quad (22)$$

which contributes a repulsive component to the total pressure. This finite-coupling correction can be used only at sufficiently large couplings and small wall separations where the correction term itself is small, *i.e.* where the $1/\Xi$ -expansion scheme remains valid. One may estimate the regime of validity of this expansion (and thus the regime of applicability of the SC theory) at a *finite* coupling parameter from Eqs. (21) and (22) as [69]

$$\left(\frac{\Delta}{\mu}\right)^2 < \Xi. \quad (23)$$

This estimate in fact agrees with our qualitative discussion in Section IV B, which predicts the strong-coupling attraction for small wall separation compared with the lateral distance of counterions, a_{\perp} , that is for

$$\Delta < a_{\perp}, \quad (24)$$

which in units of the Gouy-Chapman length (and using Eq. (5)) reproduces Eq. (23). Note also that the equilibrium wall separation predicted by the SC theory, $\Delta_{*}/\mu = 2$ (Eq. (16)), fulfills the above criterion for $\Xi > 4$.

Equation (24)—or (23) in rescaled units—is also known as the *Rouzina-Bloomfield criterion* [61], which is established as a generic attraction criterion for highly-charged macroions including charged spheres and cylinders [30, 32, 33, 41, 71].

The above discussions may be summarized in a diagram as shown in Figure 6a specifying the range of parameters (coupling parameter and the wall separation) where the strong-coupling or the mean-field picture prevails. As seen there appears a gap in the diagram, where neither of the theories can be extended to include finite-coupling effects via the series-expansion methods mentioned before. The physical situations to which this gap corresponds have been illustrated in Figures 6b and 6c (compare these Figures with Figure 4). Figure 6b shows a system in which the Gouy-Chapman length is the smallest length scale and the wall separation is large such that $\mu < a_{\perp} < \Delta$. In units of the Gouy-Chapman length, we have $1 < \Xi < (\Delta/\mu)^2$. In this case, the PB approach is not valid and in a rough approximation, the two layers are decoupled and each layer is separately described by the strong-coupling density profile for a single wall. Yet a systematic theory for the effective interaction in this regime is missing. Figure 6c shows a system in which the Gouy-Chapman length is the largest length scale and $a_{\perp} < \Delta < \mu$, or in units of the Gouy-Chapman length, $\Xi < (\Delta/\mu)^2 < 1$. In this case, counterions form a confined gas with local three-dimensional correlations for finite Ξ . Interestingly in this regime both SC theory and PB theory agree on the leading level but again have different corrections [69].

V. THE ROLE OF DIELECTRIC JUMP AT CHARGED SURFACES

So far we have assumed that the dielectric constant is uniform in space and equal for both solvent medium (where counterions are present) and charged surfaces. However, charged surfaces (macroions) usually have a dielectric constant, which is different from that of an aqueous solvent; for bio-soft materials, the dielectric constant, ϵ' , is usually

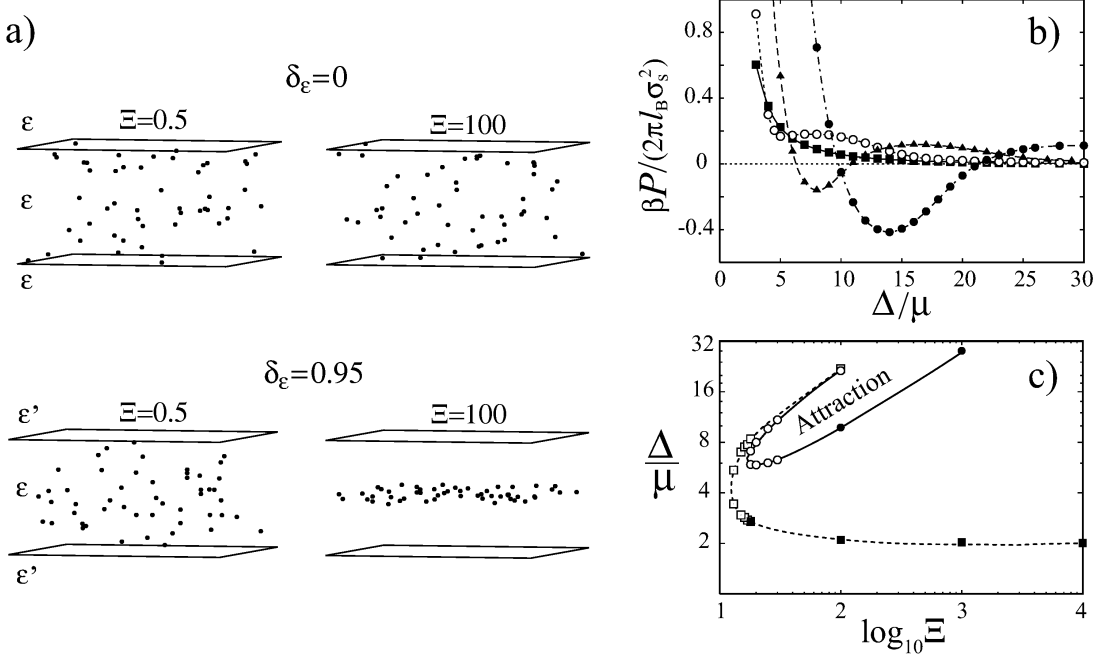


FIG. 7: a) Snapshots from MC simulations of two like-charged walls and counterions with ($\delta_\varepsilon = 0.95$) and without ($\delta_\varepsilon = 0$) a dielectric jump at the walls and for two different coupling parameters as indicated on the graph. The distance between the walls is $\Delta/\mu = 1.0$. The figure shows the main simulation box, which is replicated periodically in lateral directions in the simulation model. The lateral box size is determined from the global electroneutrality condition as $L/\mu = \sqrt{\pi \Xi N}$, where N is the number of counterions (here $N = 50$). For the sake of representation, the extension of the system in lateral directions is rescaled in each case with L/μ .

b) The rescaled effective pressure between two like-charged walls as a function of the rescaled wall separation, Δ/μ , as obtained from simulations in the presence of a dielectric jump of $\delta_\varepsilon = 0.95$ at both walls. Symbols correspond to different coupling parameters $\Xi = 0.5$ (filled squares), 10 (open circles), 30 (filled triangles), and 100 (filled circles), and connecting lines are guides to the eye.

c) Global behavior of pressure between the walls shown in terms of the rescaled wall distance, Δ/μ , and the coupling parameter, Ξ . Symbols are the zero pressure points; filled symbols show the stable bound state of the walls and open symbols show the meta-stable and unstable states [88]. Circles correspond to the case with a dielectric jump of $\delta_\varepsilon = 0.95$ at the walls, and squares represent the results for $\delta_\varepsilon = 0$ (corresponding to Figure 5b).

smaller than that of water $\varepsilon \approx 80$ (e.g. $\varepsilon' \approx 2$ for hydrocarbon). This introduces a dielectric jump at charged boundaries, which can be treated theoretically using the method of image-charges.

For a counterion of charge valency q at a charged wall of dielectric constant ε' , the image-charge is given by $q' = q\delta_\varepsilon$, where

$$\delta_\varepsilon = \frac{\varepsilon - \varepsilon'}{\varepsilon + \varepsilon'}, \quad (25)$$

uniquely represents the dielectric jump. Intuitively, one expects that a dielectric jump of $\delta_\varepsilon > 0$ leads to the depletion of counterions from the vicinity of the charged wall, since the image-charges have the same sign as counterions [21, 43, 47, 48, 94]. The depletion of counterions at a charged wall appears to be weak for small coupling parameters (the mean-field regime) and becomes significant for increasing coupling parameter (see below) [87, 94]. The counterionic density profile for $\delta_\varepsilon > 0$ shows a similar cross-over behavior as in the case of $\delta_\varepsilon = 0$ (Section III C) when coupling parameter is finite, *i.e.* it agrees with the strong-coupling prediction at small distances from the wall and follows the mean-field prediction for large distances (note that the strong-coupling theory in this case explicitly includes the image-charges). We shall not consider the case of a single charged wall here and only focus on Monte-Carlo results for the effective interaction between two like-charged walls in the presence of a dielectric jump [88].

Let us consider two like-charged walls of surface charge density $-\sigma_s$ and point-like neutralizing counterions confined in the space between the walls, which are located at a distance of Δ . We assume the same dielectric jump of $\delta_\varepsilon > 0$ at both walls. In this case, one has to account for an infinite number of image-charges for each counterion, which leads to quite involved numerical calculations. We shall therefore proceed with an approximate description by taking into account only the first-order images (that is one image for each counterion in each wall). We show typical snapshots

from Monte-Carlo simulations of the two-wall system with and without a dielectric jump in Figure 7a. The depletion of counterions from the walls is clearly seen in these snapshots and appears to be stronger for larger coupling strength, since the repulsive interaction between counterions and their images grows with Ξ . The effective pressure between the walls is shown in Figure 7b for a dielectric jump of $\delta_\varepsilon = 0.95$ (corresponding to water-hydrocarbon interface) for various coupling parameters. The image-charge interactions lead to a higher pressure at small wall separations as compared to the case with $\delta_\varepsilon = 0$ (Figure 5a). Also the range of distances at which the two walls attract each other is pushed to larger wall separations, which is more noticeable for larger coupling strength and implies a larger attraction at intermediate distances (see also Ref. [21]). However for sufficiently large wall separations, the dielectric effects weaken and the pressure becomes repulsive.

The global behavior of the effective pressure is shown in Figure 7c for $\delta_\varepsilon = 0.95$ (circles) and $\delta_\varepsilon = 0$ (squares), where symbols show the points of zero pressure with filled symbols representing the stable bound state of the walls and open symbols representing the meta-stable or unstable states (corresponding to the local minimum and maximum of the free energy). As seen, the onset of attraction is shifted to somewhat larger coupling parameters ($\Xi \approx 30$) in the presence of a dielectric jump, and also the bound state separation between the walls is larger and increases with the coupling parameter. However, one should be careful in drawing conclusions for the phase behavior of this system from the present data, since we have only considered the first-order images. The full numerical analysis of this system and comparison with extended strong-coupling theory (incorporating the dielectric jump) will be presented elsewhere [88].

VI. THE ROLE OF CURVATURE: CYLINDRICAL AND SPHERICAL MACROIONS

In the preceding Sections, we considered planar systems, whereas in realistic situations, charged surfaces often have an intrinsic curvature. For simplicity, let us consider here only charged spherical and cylindrical macroions which are characterized by a single radius of curvature R . The radius of curvature sets a new length scale, which can introduce new features in terms of counterionic properties of the system.

Intuitively, one may expect that when the radius of curvature of macroions is larger than the Gouy-Chapman length, $R \gg \mu$, the properties of the system remain *qualitatively* close to those of planar charge walls. The qualitative deviations from planar case may thus be expected for small R/μ . As we shall see later, the geometrical symmetries of macroions, *e.g.* whether they be cylindrical or spherical, also play a role as they enforce the boundary conditions to which counterions are electrostatically coupled. Still it is useful to consider the dimensionless ratio of curvature radius, R , and the Gouy-Chapman length, μ , as

$$\xi = \frac{R}{\mu}, \quad (26)$$

which can characterize some important aspects associated with the curvature. For curved surfaces of uniform surface charge density σ_s , we adopt the same definition for the Gouy-Chapman length as in Eq. (3), *i.e.*

$$\mu = \frac{1}{2\pi q\ell_B \sigma_s} = \begin{cases} R/(q\ell_B \tau) & \text{charged cylinders,} \\ 2R^2/(q\ell_B Z) & \text{charged spheres,} \end{cases} \quad (27)$$

where $\tau = 2\pi\sigma_s R$ is the linear charge density (in units of the elementary charge e) in the case of charged cylinders, and $Z = 4\pi\sigma_s R^2$ is the total charge valency for charged spheres. It is important to note that in these cases, μ does not necessarily reflect the mean distance of counterions from the surface in contrast to the charged walls.

For charged *cylinders*, the parameter ξ is quite well-known and is referred to as *Manning parameter* [89], which may be written as

$$\xi = \frac{R}{\mu} = q\ell_B \tau, \quad (28)$$

where we have used Eqs. (26) and (27). By analogy we shall refer to the same ratio for charged *spheres* as Manning parameter, which reads

$$\xi = \frac{R}{\mu} = \frac{q\ell_B Z}{2R}. \quad (29)$$

Note that in a system with counterions of finite diameter, σ_{ci} , the effective Gouy-Chapman length is larger than what one obtains for the same system with point-like counterions. Specifically, when counterions have a hard-core volume interaction with macroions, one has to use the hard-core radius of macroions in Eq. (27), that is

$$R_{hc} = R + \sigma_{ci}/2, \quad (30)$$

which is larger than the actual radius, R , resulting in a reduced surface charge density for a given Z (or τ) in the case of spheres (or cylinders). This leads to a larger Gouy-Chapman length, Eq. (27), and a smaller coupling parameter, Eq. (4). But the Manning parameter as defined in Eq. (26) remains unchanged [71].

A. Binding-unbinding transition of counterions

The peculiar features emerging in the presence of charged curved surfaces are related to the behavior of counterion at large distances from the surface. At equilibrium, counterions tend to diffuse away from macroions in order to maximize the entropy of the system, while at the same time, they are attracted energetically toward the macroion surfaces.

For counterions at a charged *sphere*, the gain in entropy grows with the distance of counterions from the macroion center, r , qualitatively as $\sim \ln r$ for large distances. The energetic attraction, on the other hand, behaves like $1/r$, which therefore is always weaker than the *entropic repulsion* experienced by counterions. Hence, counterions at a charged sphere tend to unbind completely and diffuse to infinity in the absence of confining boundaries. Thus the role of confinement becomes important in keeping counterions in the proximity of charged spheres. The confinement volume per sphere is related inversely to the concentration of spherical macroions in a solution. The qualitative considerations given above indicate that in the *infinite-dilution limit* (where the concentration of spheres tends to zero), the equilibrium counterionic density profile vanishes due to the *complete de-condensation* of counterions. Note that for a charged *wall*, the counterion-wall attraction grows linearly with distance, $\sim z$, overcoming the entropic contribution. The charged wall thus binds all its counterions, which is reflected by the fact that the density profile of counterions—though extended to infinity as in the mean-field regime—is normalizable to the total number of counterions (see Sections III A and III B). We shall investigate these aspects further in the context of interaction between two spheres in Section VII.

The case of charged *cylinders* lies between the two cases of charged walls and spheres in that the energetic attraction of counterions to the cylinder grows logarithmically with the distance from the cylinder axis, r , *i.e.* in the same way as the entropic gain increases, $\sim \ln r$. The competition between these two effects can result in a threshold binding-unbinding process in this geometry when the infinite-dilution limit is reached. In order to determine the threshold, one needs to consider the prefactor of both logarithmic contributions. The energetic attraction of a counterion to an infinitely long cylinder is given by $\beta U = 2q\ell_B\tau \ln r = 2\xi \ln r$ (per $k_B T = \beta^{-1}$). The entropic gain at large separations may be written as $S/k_B = 2 \ln r$, since the cylindrical boundary implies a two-dimensional geometry. Comparing the two contributions, a threshold value of $\xi_* = 1$ is obtained: for Manning parameter $\xi > 1$, the attraction wins and can lead to *partial* binding of counterions (with a finite density profile at the cylinder), whereas for $\xi < 1$, complete de-condensation of counterions is expected. This qualitative picture is actually supported by existing analytical results of mean-field [89, 90] and strong-coupling [71] theory; both limiting theories give the same threshold of $\xi_* = 1$. Recent numerical simulations [91] show that this threshold is in fact universal and holds in all ranges of the coupling parameter Ξ . Moreover, the threshold counterion-condensation process at charged cylinders exhibits a set of scaling relations, which are characterized by universal exponents [91].

In the case of two charged cylinders, the threshold process is expected to occur at Manning parameter $\xi = 1/2$ [78] as we shall discuss in Section VIII.

B. Attraction criteria for interacting spheres and cylinders

The binding-unbinding behavior of counterions can drastically affect the effective interaction between macroions in solution, particularly, at low concentrations of macroions. When counterionic clouds at macroions become diluted due to the de-condensation process, counterion-mediated interactions are weakened and the effective interaction between macroions is dominated by their bare Coulombic repulsion. As mentioned above, the de-condensation process may in principle occur in all ranges of the coupling parameter, Ξ , since it is regulated by the Manning parameter, ξ , which is independent from the coupling parameter. Thus for curved surfaces—in contrast to planar systems—a large coupling parameter ($\Xi \gg 1$) by itself does not necessarily indicate the regime of large electrostatic correlations, where strong-coupling attraction is expected between like charges.

In order to specify the attraction-dominated regime for interacting spheres and cylinders, one can still employ a criterion similar to the Rouzina-Bloomfield criterion introduced for two charged walls (see below). But such a criterion should be supplemented by an additional condition on Manning parameter guaranteeing that a sufficiently large fraction of counterions condense in the vicinity of macroions. It is however difficult to establish this latter condition even for the simplest interesting cases of two spheres and two cylinders. Because it requires a detailed analysis of the binding-unbinding process of counterions in these systems, which is available only in the asymptotic

cases of mean field ($\Xi \rightarrow 0$) [78, 89] and strong coupling ($\Xi \rightarrow \infty$) [71]. The mean-field theory is irrelevant for our purpose (as it does not include correlations), but as we shall see in Sections VII and VIII, the strong-coupling theory can be used to obtain a quantitative prediction for the range of Manning parameters, where attraction may occur between macroions. In the following, we briefly mention the Rouzina-Bloomfield attraction criteria for spheres and cylinders assuming that the condition on Manning parameter is fulfilled.

1. Like-charged spheres

When counterions are highly condensed at spheres, we expect that correlation effects become dominant when the typical distance between counterions, a_{\perp} , becomes much larger than the Gouy-Chapman length. Using the local electroneutrality condition, one may estimate a_{\perp} as

$$a_{\perp} \approx R \sqrt{\frac{4q}{Z}} \quad (31)$$

(up to some numerical prefactor of the order unity), which also gives a measure of the correlation hole size around counterions at surface (Figure 8). Note that in units of the Gouy-Chapman length, μ , we have $\tilde{a}_{\perp} = a_{\perp}/\mu \sim (2\Xi)^{1/2}$, where the coupling parameter for charged spheres may be written as

$$\Xi = \frac{q^3 \ell_B^2 Z}{2R^2}, \quad (32)$$

using Eqs. (4) and (27). The correlation-induced attraction is expected when the surface-to-surface distance between spheres, Δ , becomes smaller than the counterionic separation at the opposing surfaces, *i.e.*

$$\Delta < a_{\perp}. \quad (33)$$

In units of the Gouy-Chapman length, the above criterion may be written in terms of the coupling parameter as $(\Delta/\mu)^2 < \Xi$, which is qualitatively similar to the attraction condition obtained for two charged walls in Section IV C 2. The above attraction criterion was explicitly verified in simulations by Allahyarov *et al.* [30] and Linse *et al.* [32, 33] on like-charged spheres (Section VII A).

2. Like-charged cylinders

For charged (parallel) cylinders, the attraction is similarly expected to arise for

$$\Delta < a_z, \quad (34)$$

where Δ is the surface-to-surface distance of cylinders and a_z is the typical separation between condensed counterions [41]. In the case of highly-charged cylinders, counterions tend to accumulate in the intervening region between cylinders, where they line up on opposing surfaces along the cylinder axis forming a correlated inter-locking pattern [40]. The typical separation between counterions in this situation, a_z , may be estimated from the local electroneutrality condition $q = \tau a_z$, giving

$$a_z = \frac{q}{\tau}, \quad (35)$$

which agrees with the results obtained in recent simulations [40]. We shall discuss the application of criterion (34) in Section VIII B using numerical simulations of the two-cylinder system.

VII. ATTRACTION BETWEEN LIKE-CHARGED SPHERES

A. Numerical simulations

Recently, there have been several simulations [28, 29, 30, 32, 33, 34, 35] investigating effective electrostatic attraction between like-charged spheres in the large coupling regime using multivalent counterions or in some cases, using low

Simulation	q	Z	$\ell_B(\text{\AA})$	$R(\text{\AA})$	$\sigma_{ci}(\text{\AA})$	$L(\text{\AA})$	$\mu(\text{\AA})$	ξ	Ξ	$\xi_c^{(1)}$	$a_{\perp}(\text{\AA})$	$\Delta_{\text{sim}}(\text{\AA})$	$\Delta_*(\text{\AA})$
Gr{\o}nbech-Jensen <i>et al.</i> [28]	2	10	7.01	7	3.3	50-200	1.07	8.1	26	2.8-3.7	7.7	2.5	3.41
Wu <i>et al.</i> [29]		20	7.14	10	4	100	1.01	11.9	28	3.3	7.5	4	4.10
Allahyarov <i>et al.</i> [30]	2	32	112	48.9	4.4	$\sim 10^2$	0.73	70.1	615	~ 3.3	25.5	—	4.41
Linse <i>et al.</i> [32, 33]	3	60	7.15	20	4	$\sim 10^2$	0.75	29.2	85	~ 3.3	9.8	4	4.05
Hribar <i>et al.</i> [34]	3	12	7.15	10	2	$\sim 10^2$	0.94	11.7	68	~ 3.3	11.0	—	2.09

TABLE II: Parameters from simulations on highly-charged spheres: q is the charge valency of counterions with diameter σ_{ci} , Z is the charge valency of spheres with radius R , and ℓ_B , μ , ξ and Ξ are the Bjerrum length, Eq. (1), Gouy-Chapman length, Eq. (27), the Manning parameter, Eq. (29), and the coupling parameter, Eq. (32), respectively. L is the confinement box size and $\xi_c^{(1)}$ is the estimated attraction threshold discussed in Section VII C. The last two columns show the equilibrium surface-to-surface distance obtained in these simulations, Δ_{sim} (if explicitly measured), and the corresponding result from the strong-coupling theory, Δ_* . Some of the numbers are given up to the order of magnitude, and the extracted values of Δ from simulations have a typical resolution of about 1\text{\AA}. Note also that in estimating the values of Ξ , μ and a_{\perp} , we account for the finite size of counterions by assuming that they have a hard-core interaction with macroions [29, 30, 32, 33, 34]—see the note before Section VI A and Ref. [71].

dielectric constants [30] or considering the system at low temperatures [35]. Like-charge attraction is reported in all these simulations for moderate to large coupling parameters (see Table II).

The strength of attractive force obtained between spheres is sufficiently large that it can lead to closely-packed bound states (including large aggregates) between like-charged spheres [28, 29, 30, 32, 33, 34, 35]. The bound-state corresponds to an attractive minimum in the potential of mean-force between spheres at small surface-to-surface separations [28, 29, 32, 33]. An interesting feature is that the attraction regime at small separations is separated by a pronounced *potential barrier* from a repulsion regime at large separations (see Fig. 1 in Ref. [28]). On the other hand, the attractive minimum and the potential barrier are not robust and exhibit a dependence upon the size of the confinement volume [28]: for increasing confinement volume, the depth of the attractive minimum and at the same time the height of the potential barrier, decreases leading to a long-ranged repulsion between spheres in a sufficiently large confinement as expected. Though such a dependence on confinement volume appears to be quite weak (Section VII C).

The existence of a potential barrier in the interaction potential of *confined* spheres can result in meta-stable bound states between two highly-coupled spheres [35] and also indicates a first-order phase transition (phase separation between a dilute and an aggregated phase) in the thermodynamic limit [28, 32, 33].

We shall mainly focus on the attraction regime at small separations, where the attractive force between spheres maintains a typical *equilibrium* surface-to-surface distance of the order of the counterion diameter [28, 29, 32, 33]. This equilibrium (or bound-state) separation may be obtained from the location of the minimum of the potential of mean force or equivalently from the pair distribution function of spheres.

In Table II, we show the estimated values for the equilibrium surface-to-surface distance between spheres in these simulations, Δ_{sim} , along with other parameters such as the coupling parameter, Ξ , the Gouy-Chapman length, μ , as well as the estimated typical separation between counterions, a_{\perp} , from Eq. (31). As seen the Gouy-Chapman length is quite small in these systems ($\mu \sim 1\text{\AA}$) compared with the counterion separation at spheres, a_{\perp} , resulting in a large coupling parameter. The strong-coupling attraction criterion (33) is also fulfilled, since the equilibrium separation between spheres, Δ_{sim} , is found to be smaller than a_{\perp} . These observations suggest that the asymptotic strong-coupling theory is indeed relevant in the regime of parameters considered in these simulations. In the following, we shall present the strong-coupling predictions and compare them with the simulation results.

B. Effective sphere-sphere interaction: Asymptotic strong-coupling theory

Let us consider a system of two like-charged spheres (Figure 8) that are in general confined in a cubic box of edge size L inside which the global electroneutrality condition is satisfied, *i.e.* $Nq = 2Z$, where N is the number of counterions and $Z = 4\pi R^2 \sigma_s$ is the (absolute value of the) charge valency of each sphere. We assume that counterions (of diameter σ_{ci}) have also a hard-core excluded-volume interaction with the spheres.

We are interested in the limit of large couplings. As mentioned in Section IV B, the leading contribution to the free energy for $\Xi \rightarrow \infty$ involves only the one-particle contributions. The strong-coupling free energy for the two-sphere

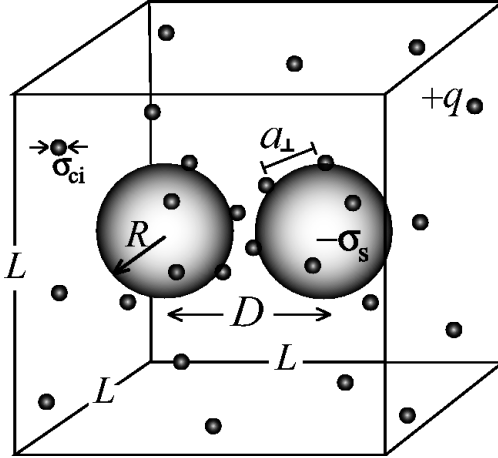


FIG. 8: Two identical like-charged spheres of radius R are considered at center-to-center distance of D in a cubic box of edge size L . The bare charge of spheres with uniform surface charge density $-\sigma_s$ (in units of the elementary charge, e , and assumed to be negative) is compensated by the total charge of counterions of charge valency q (and diameter σ_{ci}).

system may be written as (up to an irrelevant additive term) [71]

$$\frac{\beta\mathcal{F}_{SC}}{N} = \frac{\xi^2}{\tilde{D}} - \ln \int_V dx dy dz e^{-\beta u(x,y,z)}, \quad (36)$$

where $\tilde{D} = D/\mu$ is the center-to-center distance of spheres in units of the Gouy-Chapman length. The first term in Eq. (36) is the bare Coulombic repulsion of spheres with Manning parameter ξ . In the second term, βu is the single-particle interaction energy of counterions with the spheres,

$$\beta u = -2\xi^2 \left(\frac{1}{\tilde{r}_1} + \frac{1}{\tilde{r}_2} \right), \quad (37)$$

in which $\tilde{r}_1 = r_1/\mu$ and $\tilde{r}_2 = r_2/\mu$ are the rescaled radial distances from the centers of the two spheres labeled 1 and 2 (we choose the frame of reference in the middle of the box such that $r_{1,2} = [(x \pm D/2)^2 + y^2 + z^2]^{1/2}$). The spatial integral in Eq. (36) runs over the volume accessible for counterions, *i.e.* inside the cubic box excluding the two spheres (note that a shell of thickness $\sigma_{ci}/2$ around each sphere is also excluded due to the hard-core interaction between spheres and counterions).

The energetic and entropic contributions from counterions enter on the leading order through the second term in Eq. (36). It is important to note that the main qualitative features regarding the binding-unbinding behavior of counterions is reproduced by this term. In particular, for very large confining box $L \rightarrow \infty$, the single-particle partition function $\mathcal{Z}_1(D, \xi, L) = \int_V d^3r \exp(-\beta u)$ diverges with the box volume as $\mathcal{Z}_1 \sim V = L^3$ for any given Manning parameter (since the integrand is always positive and bigger than one). Thus the distribution of counterions around the spheres, $\sim \exp(-\beta u)/\mathcal{Z}_1$, as well as the component of the force contributed by counterions, $\sim \partial \ln \mathcal{Z}_1 / \partial D \sim L^{-2}$, vanish in the limit $L \rightarrow \infty$. This leads to a pure repulsion between unconfined spheres as expected. Note that this repulsion regime does not represent the strong-coupling situation associated with large electrostatic correlations. The fact that both the de-condensation process and the repulsive regime for unconfined spheres are consistently captured by the asymptotic strong-coupling free energy indicates that the $1/\Xi$ -expansion scheme used to obtain the asymptotic contribution for $\Xi \rightarrow \infty$ [69] is not only based on energetic considerations, and can also account for entropic effects on the leading order [69, 71].

Now let us consider the spheres in a finite confinement volume and investigate the strong-coupling prediction for the interaction free energy (36). For small Manning parameters, the free energy exhibits only a long-range repulsion (Figure 9a), but as Manning parameter exceeds a threshold value of $\xi_c^{(1)}$, a local minimum is developed at small separations indicating a short-range attraction and a meta-stable bound state. As seen (Figures 9b and c), this attraction regime is separated from the large-distance repulsion regime by a pronounced potential barrier. For increasing Manning parameter, the attractive local minimum becomes deeper than the large-distance minimum, and the potential barrier disappears beyond a second threshold of $\xi_c^{(2)}$ —see Figure 9d. The preceding features indicate a discontinuous unbinding transition between a closely-packed bound-state and a repulsion-dominated state of two like-charged spheres by varying the Manning parameter. The generic form of the free energy also agrees qualitatively with numerical findings [28] as discussed in Section VII A.

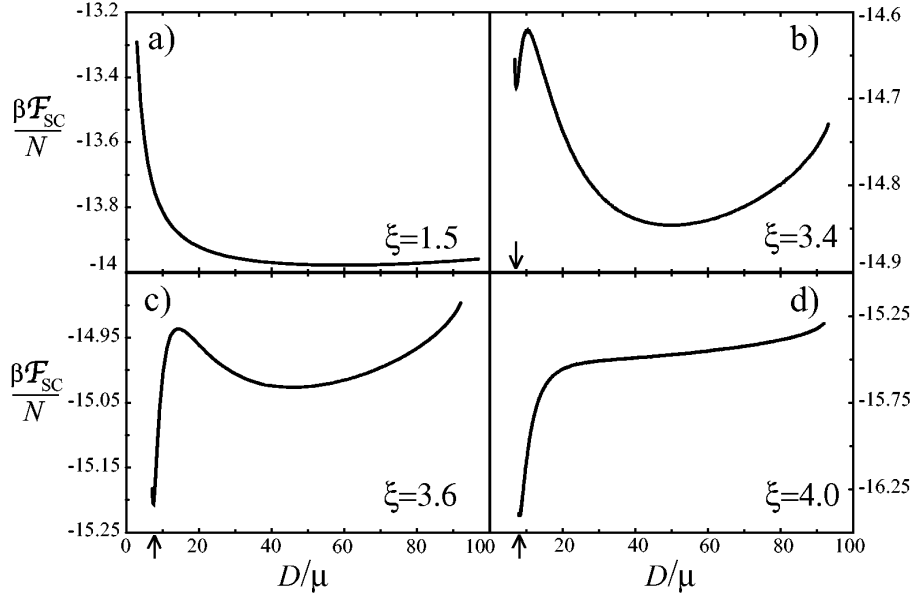


FIG. 9: The strong-coupling free energy of the two-sphere system, Eq. (36), plotted as a function of the rescaled center-to-center distance, D/μ , for Manning parameters a) $\xi = 1.5$, b) $\xi = 3.4$, c) $\xi = 3.6$ and d) $\xi = 4.0$ (the box size is $L/\mu = 100$). The location of the local minimum at small separations is marked by an arrow. A potential barrier is found in the range of Manning parameter $\xi_c^{(1)}(L) < \xi < \xi_c^{(2)}(L)$, where we have $\xi_c^{(1)} \approx 3.3$ and $\xi_c^{(2)} \approx 3.8$ for $L/\mu = 100$. The values of the two free energy minima become equal at $\xi \approx 3.5$.

A diagram representing different regimes of attraction and repulsion is shown in Figure 10, where we have plotted the locations of the minima (solid curves) of the strong-coupling free energy (36) and also the location of its maximum (dashed curves) as a function of Manning parameter, ξ . (The locations of the two threshold Manning parameters, $\xi_c^{(1)}$ and $\xi_c^{(2)}$, are shown by arrows.) One can show that for $\xi \ll 1$, the location of the repulsion-dominated minimum at large separations (Figure 9a), D_* , scales linearly with the box size as

$$D_* \approx \sqrt[3]{\frac{3}{4\pi} L}, \quad (38)$$

when the box size tends to infinity $L \rightarrow \infty$ [71]. On the other hand, for large Manning parameter $\xi \gg 1$, the location of the attraction-dominated minimum at small separations (Figure 9d), D_* , saturates to a value independent from the box size; in this case, the equilibrium surface-to-surface distance of spheres, $\Delta_* \equiv D_* - 2R$, follows from Eq. (36) approximately as

$$\Delta_* \equiv D_* - 2R \approx \sigma_{ci} + \frac{4}{7}\mu + \mathcal{O}(\mu^2), \quad (39)$$

where σ_{ci} is the counterion diameter. This minimum corresponds to a highly-condensed state of counterions in the intervening region between spheres [71]. The attractive force induced between spheres in this regime ($\xi \gg 1$) may also be calculated from the strong-coupling free energy (36); at small separations ($D \sim 2R$), the force takes the following analytical form

$$F(D) \approx -7 \frac{Z^2 e^2}{4\pi\epsilon\epsilon_0 D^2}. \quad (40)$$

This limiting attractive force (for $\Xi \gg 1$ and $\xi \gg 1$) is independent from the temperature and results only from energetic contributions [71]. The expression (40) qualitatively agrees with the results obtained by Shklovskii using the Wigner-crystal model [65].

The predictions of the strong-coupling theory for the bound-state separation of two attracting spheres, Δ_* , has been compared with numerical simulations in Table II (note that here Δ_* has been calculated by numerical evaluation of the free energy (36) for the corresponding simulation parameters. The analytical expression (39) may also be used, but it gives an approximate value up to the first order in μ). As seen there is a reasonable semi-quantitative agreement

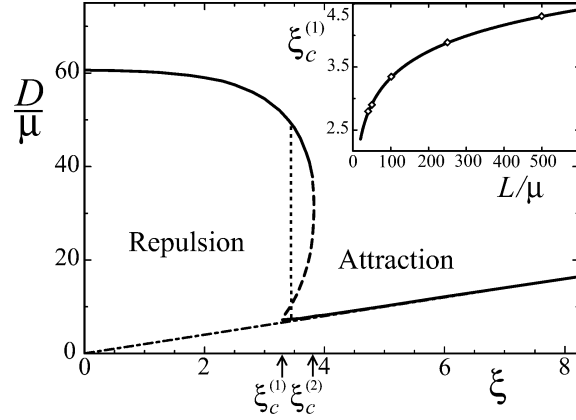


FIG. 10: Regimes of attraction and repulsion in the system of two like-charged spheres and counterions as obtained from the asymptotic strong-coupling theory. The solid curves show the rescaled equilibrium center-to-center distance between spheres as a function of the single-sphere Manning parameter, ξ (Eq. (29)), for a confining box of rescaled size $L/\mu = 100$. The dashed curve corresponds to the maximum of the strong-coupling free energy and the dotted vertical line shows the Manning parameter for which the values of the two minima of the free energy are equal (see Figure 9). The locations of threshold Manning parameters $\xi_c^{(1)}$ and $\xi_c^{(2)}$ are shown by arrows. The dot-dashed line shows the contact separation $D = 2R$. Inset: The attraction threshold for two like-charged spheres, $\xi_c^{(1)}$, increases weakly with the rescaled box size, L/μ . It exhibits a logarithmic dependence according to Eq. (42), which is shown by the solid curve.

between the theoretical predictions and the simulation results. As mentioned in Section VII A, the equilibrium surface-to-surface distance in these simulations appears to be about the counterion diameter (see the Discussion in Ref. [33]). This also follows from the strong-coupling prediction, Eq. (39), since for highly-charged spheres, the Gouy-Chapman length is in fact small compared with the counterion diameter. One should also note that the lateral separation of counterions at spheres in the simulations is typically larger than the counterion diameter indicating that the excluded-volume interaction between counterions is not a dominant effect. The volume interactions between counterions enter only in the higher-order corrections to the asymptotic theory and can lead to additional attractive components between macroions [30, 40].

C. Attraction threshold

The strong-coupling theory also allows to obtain an analytical estimate for the regime of Manning parameters where attraction is expected between spheres. This regime may be specified by

$$\xi > \xi_c^{(1)}, \quad (41)$$

where the threshold Manning parameter $\xi_c^{(1)}$ actually depends on the confinement size, $\xi_c^{(1)} = \xi_c^{(1)}(L)$. As shown in the inset of Figure 10, $\xi_c^{(1)}(L)$ increases almost logarithmically with the box size as

$$\xi_c^{(1)}(L) \approx a + b \ln \left(\frac{L}{\mu} \right), \quad (42)$$

where $a \approx 0.55$ and $b \approx 0.6$ are obtained by fitting to numerically-determined SC predictions (symbols). The estimated values of $\xi_c^{(1)}$ are shown in Table II for the given simulation parameters, which show that these simulations indeed exhibit the attraction regime (41). The weak dependence of the attraction threshold, $\xi_c^{(1)}$, on the confinement size can also explain the stability of compact clusters of spheres in quite large confinements ($L/\mu \gg 1$) [28, 29, 30, 32, 33, 34, 35], since the Manning parameter only needs to exceed a moderate value ($\sim \ln L/\mu$) for like-charged spheres to fall into the attraction-dominated regime.

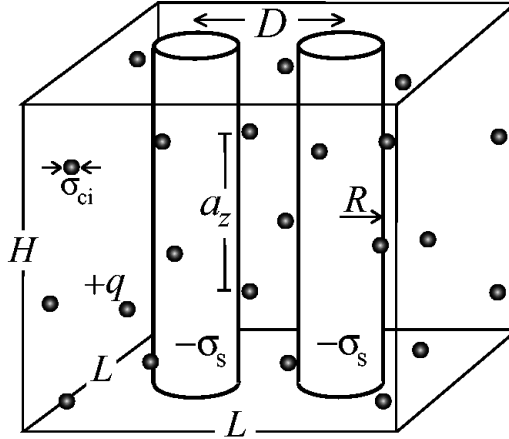


FIG. 11: Two identical and parallel charged cylinders of radius R are considered at axial separation of D and in a square box of lateral edge size L ; cylinders have a length of H , which is assumed to be infinitely large. The bare charge of cylinders with uniform surface charge density $-\sigma_s$ (in units of the elementary charge, e , and assumed to be negative) is compensated by the total charge of counterions of charge valency q (and diameter σ_{ci}).

VIII. ATTRACTION BETWEEN LIKE-CHARGED CYLINDERS

A. Effective cylinder-cylinder interaction: Asymptotic strong-coupling theory

In this Section, we shall consider the interaction between two like-charged cylinders in the limit of large coupling parameter $\Xi \rightarrow \infty$. For simplicity, we assume that the cylinders are infinitely long (with length H), and that they are confined in a square box of edge size L (see Figure 11). The electroneutrality condition holds inside the confining box, thus we have $qN = 2\tau H$, where N is the number of counterions and $\tau = 2\pi\sigma_s R$ is the linear charge density of each cylinder. We assume that counterions and cylinders have also a hard-core excluded-volume interaction.

The strong-coupling free energy of this system (up to an irrelevant additive term) follows as [71]

$$\frac{\beta\mathcal{F}_{SC}}{N} = -\xi \ln \tilde{D} - \ln \int_V dx dy e^{-\beta u(x,y)}, \quad (43)$$

where $\tilde{D} = D/\mu$ is the axial separation of the cylinders in units of the Gouy-Chapman length. The first term in Eq. (43) is the bare repulsion of cylinders and in the second term, βu is the single-particle interaction energy of counterions with the cylinders,

$$\beta u = 2\xi(\ln \tilde{r}_1 + \ln \tilde{r}_2), \quad (44)$$

where $\tilde{r}_1 = r_1/\mu$ and $\tilde{r}_2 = r_2/\mu$ are the radial distances from the axes of the two cylinders (in the xy -plane perpendicular to the cylinders axes)—we choose the frame of reference in the middle of the box such that $r_{1,2} = [(x \pm D/2)^2 + y^2]^{1/2}$. The integral in Eq. (43) runs over the volume accessible for counterions inside the box excluding the two cylinders (and a shell of thickness $\sigma_{ci}/2$ around each cylinder corresponding to the closest approach distance of counterions).

As in the case of two spheres (Section VII B), the effective interaction between like-charged cylinders is influenced by the binding-unbinding behavior of counterions incorporated on the leading order in the single-particle partition function $\mathcal{Z}_1(D, \xi, L) = \int_V d^2r \exp(-\beta u)$ in the second term of the free energy (43). For further analysis of this behavior in the two-cylinder system, let us first consider the limit of very large box size $L \rightarrow \infty$. In this limit, \mathcal{Z}_1 scales with the box size as $\mathcal{Z}_1 \sim L^{2-4\xi}$, which may be seen simply by rescaling the spatial coordinates with L as $x \rightarrow x/L$, etc. Thus for $\xi < 1/2$, \mathcal{Z}_1 diverges and consequently, the distribution function of counterions, $\sim \exp(-\beta u)/\mathcal{Z}_1$, vanishes indicating de-condensation of counterions from the two cylinders. The counterion-mediated force between cylinders, $\sim \partial \ln \mathcal{Z}_1 / \partial D$, tends to zero as well; thus the cylinders only repel each other in the limit $L \rightarrow \infty$. In contrast, for Manning parameter $\xi > 1/2$, counterions bind to the two unconfined cylinders with a finite density profile, and thus can produce attraction between them. The condensation threshold obtained above for two cylinders, $\xi_* = 1/2$, agrees with the classical result due to Manning [78] quantitatively.

An interesting question is to obtain the regime of Manning parameters, where the attraction emerges between cylinders. Intuitively, we expect that the effective attraction sets in somewhat above the counterion-condensation

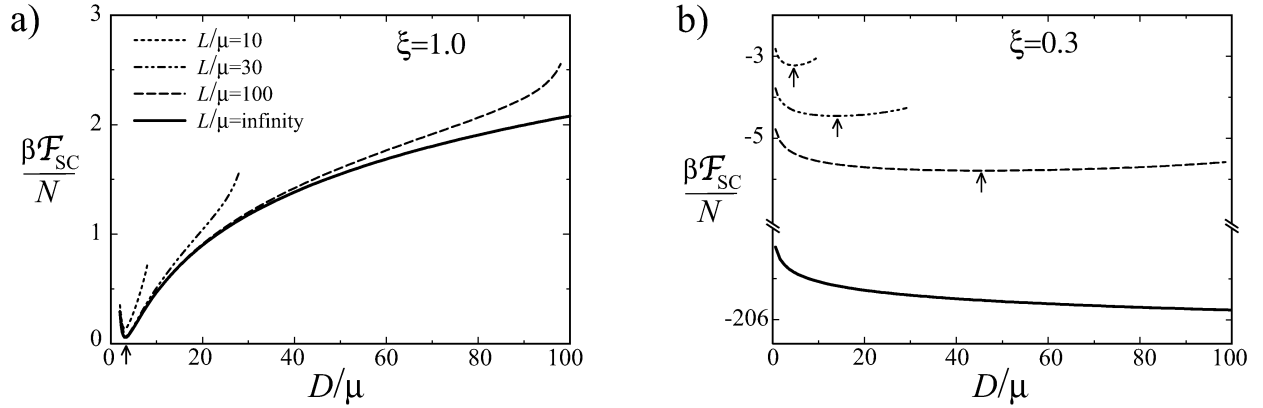


FIG. 12: The strong-coupling free energy of the two-cylinder system as a function of the rescaled axial distance, D/μ , for Manning parameters a) $\xi = 1.0$ and b) $\xi = 0.3$ and for several box sizes as indicated on the graph. Arrows show the approximate location of the minimum of the free energy, which for large Manning parameters is nearly independent of the box size and reflects a closely-packed bound state. For small Manning parameter $\xi < \xi_c = 2/3$, the location of the minimum tends to infinity with the box size reflecting a continuous unbinding transition for like-charged cylinders.

threshold $\xi_* = 1/2$. Because right at the condensation threshold, there is an unbalanced bare repulsion between the cylinders, and a finite fraction of condensed counterions is needed to compensate this repulsion. It follows from a more detailed analysis of the strong-coupling free energy (43) that the attraction actually emerges when [71]

$$\xi > \xi_c = 2/3, \quad (45)$$

which gives a universal threshold for attraction between unconfined cylinders.

The attraction threshold between two like-charged cylinders has also been investigated using other methods. Analysis of Ray and Manning [78] based on the classical counterion-condensation theory [89] predicts attraction between two like-charged cylinders for $\xi > 1/2$, which coincides with the onset of counterion condensation. It should be noted, however, that the attraction mechanism involved in their theory is not based on electrostatic correlations, but features a mean-field covalence-like binding process. Arenzon *et al.*'s study [63, 70] based on a structural-correlations theory (which also accounts for counterion condensation) predicts attraction for $\xi > 2$. Numerical simulations [27, 40, 41, 42], on the other hand, give attraction for the range of Manning parameters $\xi > 0.8$, but have not yet specified the attraction threshold precisely (Section VIII B).

For two cylinders in a finite confinement volume, one can determine the attraction and repulsion regimes by evaluating the strong-coupling free energy Eq. (43). The typical form of the free energy (43) is shown in Figure 12 for both large ($\xi > \xi_c = 2/3$) and small ($\xi < \xi_c = 2/3$) Manning parameters. For large Manning parameter (Figure 12a), the free energy exhibits a long-range attraction and a local minimum at small separations, which is quite insensitive to the confinement size as counterions are localized mostly in the proximity of the cylinders in this regime. The analytical form of the attraction force (per unit length of the cylinders H) may be estimated for large Manning parameters $\xi \gg 1$ [71]; in the zero-temperature limit ($\xi \rightarrow \infty$), we have:

$$\frac{F(D)}{H} \approx -\frac{e^2 \tau^2}{2\pi \varepsilon \varepsilon_0} \times \begin{cases} 1/D & D \gg 2R, \\ 3/D & D \approx 2R, \end{cases} \quad (46)$$

for large and small axial separations respectively. This limiting attractive force (which is obtained for $\Xi \gg 1$ and $\xi \gg 1$) is independent from the temperature and originates from a purely electrostatic origin.

For small Manning parameter $\xi < \xi_c = 2/3$ (Figure 12b), the interaction free energy of cylinders is dominated by their bare repulsion as counterionic clouds become increasingly diluted around the cylinders. The location of the minimum of the free energy for $\xi \ll 1$, D_* , tends to infinity with the box size as $D_* \approx L/\sqrt{\pi}$.

In brief, one may specify the attraction and repulsion regimes of two like-charged cylinders by considering the location of the minimum of the free energy (43) as shown in Figure 13a for several different box sizes (the region below each curve shows the repulsion regime and above that is the attraction regime). For $\xi \gg 1$, the equilibrium surface-to-surface separation of the cylinders, Δ_* , may be obtained approximately as

$$\Delta_* \equiv D_* - 2R \approx \sigma_{ci} + \frac{2}{3}\mu + \mathcal{O}(\mu^2), \quad (47)$$

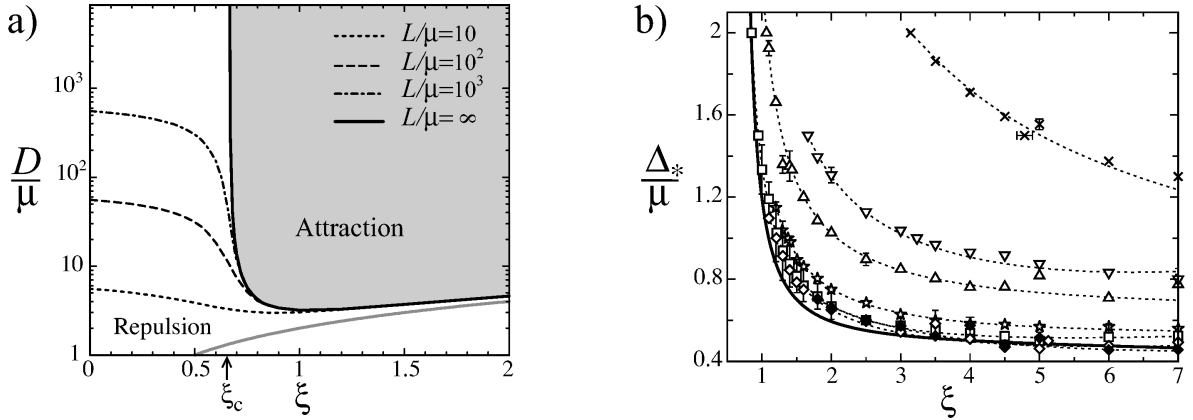


FIG. 13: a) Regimes of attraction and repulsion in the system of two like-charged cylinders and counterions as obtained from the asymptotic strong-coupling theory. The curves show the rescaled equilibrium axial separation between cylinders, D_*/μ , as a function the single-cylinder Manning parameter, ξ (Eq. (28)), for confining boxes of different size as indicated on the graph. The curves are obtained numerically by minimization of the free energy (43). In an unconfined box, the cylinders continuously unbind at the threshold Manning parameter $\xi_c = 2/3$ (shown by an arrow). The thick gray curve corresponds to $D = 2R$, where the two cylinders are at contact.

b) The rescaled equilibrium surface-to-surface separation of the cylinders, $\Delta_*/\mu = (D_* - 2R)/\mu$, as a function of Manning parameter, ξ . Symbols are simulation data for the Rouzina-Bloomfield parameter (from top): $\gamma_{RB} = 3$ (crosses), 10 (triangle-downs), 15 (triangle-ups), 30 (stars), 40 (squares), 50 (open diamonds) and 60 (filled diamonds) [41]. The solid curve is the strong-coupling prediction obtained from Eq. (43). Dashed curves are guides to the eye.

where σ_{ci} is the counterion diameter. For typical strongly-coupled systems (with small Gouy-Chapman length), the equilibrium surface separation is predicted from Eq. (47) to be of the order of the counterion diameter.

When Manning parameter decreases down to the attraction threshold $\xi_c = 2/3$, the two cylinders unbind from each other for $L \rightarrow \infty$ (solid curve in Figure 13a). But in contrast to like-charged spheres, the unbinding transition of cylinders occurs in a continuous fashion exhibiting a universal scaling exponent for the diverging axial distance of cylinders [71]

$$D_* \sim (\xi - \xi_c)^{-\alpha}, \quad (48)$$

where the exponent is found as

$$\alpha = 3/2. \quad (49)$$

B. Comparison with numerical simulations

Several numerical simulations have been reported on charged cylinders [27, 40, 41, 42] and also on more detailed models, which incorporate the charge pattern of DNA [26, 36]. Attraction is found in a wide range of Manning parameters (including $\xi \approx 1.0$) and for moderate to large coupling parameters.

Grønbech-Jensen *et al.* [27] showed that the effective interaction between two parallel like-charged cylinders in the presence of divalent counterions exhibits repulsion at very small distances close to contact and attraction at intermediate distances by means of which a closely-packed bound state is maintained at small surface separations. At large distances the effective interaction turns to repulsion. Similar results have been reported in simulations by Lee *et al.* [42]. In these simulations, charges on cylinders and counterions interact with Coulombic interactions as well as short-range excluded-volume interactions. Recent simulations by Deserno *et. al* [40] indicate an interplay between electrostatic and excluded-volume interactions, which may drastically influence the effective *electrostatic* interaction between like-charged cylinders. Specially for large linear charge densities (when charge separation on the cylinder is smaller than the counterion size), the attractive electrostatic force between cylinders weakens and eventually turns to repulsion for sufficiently large coupling strength [40]. In this case, the *total* effective force between the cylinders is still attractive due to an attractive component from excluded-volume interactions. This behavior is not yet completely understood and appears to be different from a simple depletion mechanism [40]. A similar situation may be present in the system studied in Ref. [27], however, the detailed analysis of the force components is not reported.

Intuitively, we expect that excluded-volume effects become important when typical distance between counterions on cylinders surface, $a_z = q/\tau$ (Section VI B 2), is smaller than the counterion diameter, σ_{ci} , *i.e.* for $a_z < \sigma_{ci}$. In this case, excess accumulation of counterions in the intervening region between cylinders, which is favored energetically and leads to the strong-coupling attraction [71], is prohibited [40]. In order to investigate the electrostatic features of like-charge attraction in the two-cylinder system and to avoid complications arising from volume interactions, we consider recent Molecular Dynamics simulations performed by Arnold and Holm, which exclude volume interactions between counterions though counterions still retain a soft-core excluded-volume repulsion with the cylinders [41]. This is important for the forthcoming comparison made with the strong-coupling predictions, since the leading-order results at large couplings only involve counterion-cylinder interactions (Section VIII). The simulation model has a geometry similar to what we have shown in Figure 11, where periodic boundary conditions in z direction is used. (For convenience the simulated model employs a cylindrical outer boundary of diameter $8D$. For final comparison, the theoretical curves are also calculated using a similar constraint, though for simplicity, a square box of edge size $L = 8D$ is used, which as explicitly checked does not influence the following results in the considered range of Manning parameters [41].) The soft-core repulsion in the simulations is also chosen strong enough such that it effectively prevents counterions from penetrating the cylinders, which makes the simulation model comparable to the theoretical model with a hard-core volume interaction. In the simulations, cylinders are kept at fixed surface-to-surface distance, Δ , with fixed linear charge density, τ , and counterion valency, q , but the Bjerrum length and the cylinders radius, R , are varied. Hence, the Gouy-Chapman length, μ (Eq. (27)), varies accordingly allowing to span the phase space of the system and specify the attraction and repulsion regimes.

In Figure 13b, we show the simulation results for the equilibrium surface-to-surface distance of cylinders in rescaled units, Δ_*/μ , as a function of Manning parameter $\xi = q\ell_B\tau$ (Eq. (28)). Different symbols correspond to different values of the *Rouzina-Bloomfield parameter* defined as

$$\gamma_{RB} = \frac{q}{\tau\Delta}, \quad (50)$$

which is fixed for each simulation data set. This dimensionless ratio gives a measure of the deviations from the strong-coupling regime, since it represents the ratio between the estimated correlation hole size, $a_z = q/\tau$ [40], and the surface-to-surface distance between cylinders (see Section VI B 2) [92]. Thus according to Rouzina-Bloomfield criterion, large $\gamma_{RB} = a_z/\Delta$ corresponds to a strongly-coupled system with highly correlated structures on opposite surfaces of cylinders that may give rise to attraction between them. This behavior is clearly supported by the present simulations as seen in Figure 13b. For increasing γ_{RB} (from about 3 up to 60), the equilibrium separation between cylinders decreases and tends to the strong-coupling prediction indicating a closely-packed bound state at large Manning parameters $\xi > 1$, where the equilibrium surface-to-surface distance is of the order of the Gouy-Chapman length.

The quantitative agreement with the strong-coupling prediction is obtained for the whole range of Manning parameters studied in the simulations. Due to convergence limitations, the simulations so far have been limited to the range of Manning parameters $\xi > 0.8$. It becomes more difficult to obtain good data for smaller Manning parameters as the distance between cylinders rapidly increases. Nonetheless, the excellent convergence of the present data to the strong-coupling curve suggests an attraction threshold of about $\xi_c = 2/3$ obtained in Section VIII A.

IX. CONCLUDING REMARKS AND DISCUSSION

We have discussed the effective electrostatic interaction between like-charged macroions in the regime of large coupling parameter, Ξ , which is achieved for large counterion valency, large charge densities on macroions, at low dielectric constants or low temperatures. In this regime, interactions between macroions are dominated by strong counterionic correlations: counterions form highly correlated layers at macroions, including Wigner crystals for sufficiently large coupling, that lead to attractive forces between like-charged macroions at sufficiently small surface separations. The relevant length scale is set by the typical distance between counterions at macroion surfaces (the correlation hole size) below which like-charged surfaces couple to each other electrostatically. This energetic coupling is essentially mediated by single counterions sandwiched between opposite surfaces of macroions. At larger surface separations, however, correlation effects and the attraction strength are reduced and multi-counterion interactions play a significant role. At very large separation (as long as the coupling parameter is finite), the interaction between macroions is dominated by mean-field features and eventually turns to repulsion.

The strong-coupling attraction appears with the same mechanism for planar and curved surfaces. For curved surfaces, however, attraction is found only when a sufficiently large number of counterions are condensed near the surface; the condensation process is regulated by the ratio between the radius of curvature, R , and the Gouy-Chapman length, μ , that is the Manning parameter $\xi = R/\mu$. Therefore, the attraction regime for charged cylinders and spheres

is characterized by both a large coupling parameter Ξ , which is specified via the Rouzina-Bloomfield criterion, and also by a large Manning parameter, which has to be determined by considering the condensation process of counterions in the given system of macroions (Sections VI-VIII).

We reviewed recent analytical results obtained in the limit of $\Xi \rightarrow \infty$, which gives rise to the asymptotic strong-coupling theory. This theory incorporates single-particle contributions on a systematic level and may be extended to finite coupling regimes by considering higher-order corrections via a $1/\Xi$ -expansion series (virial expansion) [69]. The predictions of the strong-coupling theory were considered for the effective interaction between two charged walls and also for two spherical and cylindrical macroions. This asymptotic theory yields a long-ranged attractive force between like-charged objects that is of constant strength for two walls, but varies with distance, D , as $\sim 1/D$ for two cylinders and as $\sim 1/D^2$ for two spheres. Note that the leading-order free energy contains in addition to energetic contributions also (repulsive) entropic contributions from counterions (see Eqs. (15), (36) and (43)), which vanish at zero temperature. The zero temperature limit is in fact contained within the strong-coupling theory and may be obtained by taking the limit $\mu \rightarrow 0$ (or $\xi \rightarrow \infty$ for curved surfaces), where the free energy reduces to a purely energetic contribution giving a long-ranged attractive force as specified above (see Eqs. (15), (40), (46) and Ref. [71]). As we know from analytical and numerical studies of planar walls [39, 69], the range of strong-coupling attraction is reduced substantially at finite couplings due to higher-order corrections. (The higher-order corrections have not yet been calculated for the system of two cylinders and two spheres.) By comparing the strong coupling predictions with recent simulations, it was shown that the attraction regime and the closely-packed bound state of macroions can be described by this limiting theory on a quantitative level [37, 38, 39, 41, 71]. Note that the agreement with simulations is limited to the regime of surface separations determined by the Rouzina-Bloomfield criterion. This regime particularly includes typical coupling parameters of $\Xi \sim 10^2$ and Manning parameters of $\xi \sim 10$ (for spheres) and $\xi > 1$ (for cylinders), which are accessible in usual experimental systems (see Tables I and II).

The asymptotic strong-coupling theory was also considered to estimate the threshold Manning parameter above which the attraction is expected for two like-charged spheres and cylinders. The attraction threshold is captured within the asymptotic theory because it accounts for the entropy-driven de-condensation process of counterions on the leading order. One should note, however, that the de-condensation regime does not involve electrostatic correlations and thus in general, the strong-coupling theory may be only qualitatively valid when counterions de-condense at *low* Manning parameters. Yet strong-coupling predictions were shown to remain in a reasonable agreement with simulations on two cylinders for decreasing Manning parameter close to de-condensation threshold [41]. (Moreover, the predicted de-condensation threshold itself agrees quantitatively with the standard Manning results for one and two cylinders [78, 89].) Further numerical and analytical studies are useful to specify the validity of the strong-coupling predictions at low Manning parameters, including the predicted unbinding behavior of cylinders and spheres.

We did not discuss possible thermodynamic phase transitions triggered by attractive forces in the system of charged plates, spheres and cylinders. (Note that the binding-unbinding behaviors discussed in Sections VII and VIII represent thermodynamic phase transitions only in the case of infinitely long cylinders; for spheres (or short cylinders) there will be additional entropic contributions to the free energy from the sphere-sphere distance coordinate, which are not considered within the present model.) A first-order unbinding transition was predicted to occur in the system of two like-charged walls at the coupling parameter $\Xi \approx 17$ that has also been compared with experimental observations [39]. Also there has been indication of an attraction-induced phase separation in the system of like-charged spheres from recent numerical simulations [27, 32, 33]. The systematic study of such phase transitions still remains a challenging subject (see Ref. [93] and references therein).

Another interesting problem is to examine the influence of additional salt on the interactions in the strong-coupling limit. The present results are expected to remain valid at sufficiently small salt concentrations (large screening length). Qualitatively, one can associate the size of the confinement box considered in the present models with the screening length. Thus, addition of salt is expected to matter particularly close to the unbinding threshold of macroions. Other relevant subjects include the effect of finite polymer stiffness, the discrete charge pattern of macroions [26, 36, 58, 62, 63, 65, 67, 94], and bundling of many charged polymers [10, 16, 31, 52, 65, 76] in the strong coupling regime, which constitute interesting applications for the future.

Acknowledgments

We acknowledge financial supports from the DFG Schwerpunkt Polyelektrolytes with defined architecture and the DFG German-French Network.

[1] E.J. Verwey, J.T.G. Overbeek, *Theory of the Stability of Lyophobic Colloids* (Elsevier, Amsterdam, 1948).

[2] J. Israelachvili, *Intermolecular and Surface Forces* (Academic Press, London, 1991).

[3] R.J. Hunter, *Foundations of Colloidal Science* (Clarendon, Oxford, 1987).

[4] D.H. Napper, *Polymeric Stabilization of Colloidal Dispersions* (Academic Press, London, 1983).

[5] H. Dautzenberg, W. Jaeger, B.P.J. Kötz, C. Seidel, D. Stscherbina, *Polyelectrolytes: Formation, characterization and application* (Hanser Publishers, New York, 1994).

[6] T.D. Yager, C.T. McMurray, K.E. van Holde, *Biochem.* **23**, 2271 (1989).

[7] A. Khan, B. Jönsson, H. Wennerström, *J. Phys. Chem.* **89**, 5180 (1985).

[8] H. Wennerström, A. Khan, B. Lindman, *Adv. Colloid Interface Sci.* **34**, 433 (1991).

[9] R. Kjellander, S. Marçelja, J.P. Quirk, *J. Colloid Interface Sci.* **126**, 194 (1988).

[10] V.A. Bloomfield, *Biopolymers* **31**, 1471 (1991); *Curr. Opin. Struct. Biol.* **6**, 334 (1996).

[11] P. Kékicheff, S. Marçelja, T. J. Senden, V. E. Shubin, *J. Chem. Phys.* **99**, 6098 (1993).

[12] M. Delsanti, J.P. Dalbiez, O. Spalla, L. Belloni, M. Drifford, *ACS Symp. Ser.* **548**, 381 (1994).

[13] P. Gonzalez-Monzuelos, M. Olvera de la Cruz, *J. Chem. Phys.* **103**, 3145 (1995); M. Olvera de la Cruz, L. Belloni, M. Delsanti, J.P. Dalbiez, O. Spalla, M. Drifford, *J. Chem. Phys.* **103**, 5781 (1995).

[14] M. Dubois, T. Zemb, N. Fuller, R.P. Rand, V.A. Parsegian, *J. Chem. Phys.* **108**, 7855 (1998).

[15] H.H. Strey, R. Podgornik, D.C. Rau, V.A. Parsegian, *Curr. Opin. Struct. Biol.* **8**, 309 (1998).

[16] J.X. Tang, S. Wong, P. Tran, P.A. Janmey, *Ber. Bunsen-Ges. Phys. Chem.* **100**, 1 (1996); J.X. Tang, T. Ito, T. Tao, P. Traub, P.A. Janmey, *Biochemistry* **36**, 12600 (1997).

[17] G.C.L. Wong, A. Lin, J.X. Tang, Y. Li, P.A. Janmey, C.R. Safinya, *Phys. Rev. Lett.* **91**, 018103 (2003); J.C. Butler, T. Angelini, J.X. Tang, G.C.L. Wong, *Phys. Rev. Lett.* **91**, 028301 (2003).

[18] T.E. Angelini, H. Liang, W. Wriggers, G.C.L. Wong, *Proc. Natl. Acad. Sci. USA* **100**, 8634 (2003).

[19] L. Guldbrand, B. Jönsson, H. Wennerström, P. Linse, *J. Chem. Phys.* **80**, 2221 (1984).

[20] B. Svensson, B. Jönsson, *Chem. Phys. Lett.* **108**, 580 (1984).

[21] D. Bratko, B. Jönsson, H. Wennerström, *Chem. Phys. Lett.* **128**, 449 (1986).

[22] L. Guldbrand, L.G. Nilsson, L. Nordenskiöld, *J. Chem. Phys.* **85**, 6686 (1986); L.G. Nilsson, L. Guldbrand, L. Nordenskiöld, *Mol. Phys.* **72**, 177 (1991).

[23] C.E. Woodward, B. Jönsson, T. Åkesson, *J. Chem. Phys.* **89**, 5145 (1988).

[24] J.P. Valleau, R. Ivkov, G.M. Torrie, *J. Chem. Phys.* **95**, 520 (1991).

[25] R. Kjellander, T. Åkesson, B. Jönsson, S. Marçelja, *J. Chem. Phys.* **97**, 1424 (1992).

[26] A.P. Lyubartsev, L. Nordenskiöld, *J. Phys. Chem.* **99**, 10373 (1995).

[27] N. Grønbech-Jensen, R.J. Mashl, R.F. Bruinsma, W.M. Gelbart, *Phys. Rev. Lett.* **78**, 2477 (1997).

[28] N. Grønbech-Jensen, K.M. Beardmore, P. Pincus, *Physica A* **261**, 74 (1998).

[29] J. Wu, D. Bratko, J.M. Prausnitz, *Proc. Natl. Acad. Sci. USA* **95**, 15169 (1998); J. Wu, D. Bratko, H.W. Blanch, J.M. Prausnitz, *J. Chem. Phys.* **111**, 7084 (1999).

[30] E. Allahyarov, I. D'Amico, H. Löwen, *Phys. Rev. Lett.* **81**, 1334 (1998).

[31] M.J. Stevens, *Phys. Rev. Lett.* **82**, 101 (1999).

[32] P. Linse, V. Lobaskin, *Phys. Rev. Lett.* **83**, 4208 (1999).

[33] P. Linse, V. Lobaskin, *J. Chem. Phys.* **112**, 3917 (2000); P. Linse, *J. Chem. Phys.* **113**, 4359 (2000).

[34] B. Hribar, V. Vlachy, *Biophys. J.* **78**, 694 (2000).

[35] R. Messina, C. Holm, K. Kremer, *Phys. Rev. Lett.* **85**, 872 (2000); *Europhys. Lett.* **51**, 461 (2000).

[36] E. Allahyarov, H. Löwen, *Phys. Rev. E* **62**, 5542 (2000).

[37] A.G. Moreira, R.R. Netz, *Europhys. Lett.* **52**, 705 (2000).

[38] A.G. Moreira, R.R. Netz, *Phys. Rev. Lett.* **87**, 078301 (2001).

[39] A.G. Moreira, R.R. Netz, *Eur. Phys. J. E* **8**, 33 (2002).

[40] M. Deserno, A. Arnold, C. Holm, *Macromolecules* **36**, 249 (2003).

[41] A. Naji, A. Arnold, C. Holm, R.R. Netz, *Europhys. Lett.* **67**, 130 (2004).

[42] K.-C. Lee, I. Borukhov, W.M. Gelbart, A.J. Liu, M.J. Stevens, *Phys. Rev. Lett.* **93**, 128101 (2004).

[43] R. Kjellander, S. Marçelja, *Chem. Phys. Lett.* **112**, 49 (1984); *J. Chem. Phys.* **82**, 2122 (1985).

[44] F. Oosawa, *Biopolymers* **6**, 1633 (1968).

[45] F. Oosawa, *Polyelectrolytes* (Marcel Dekker, New York, 1971).

[46] P. Attard, R. Kjellander, D.J. Mitchell, *Chem. Phys. Lett.* **139**, 219 (1987); P. Attard, R. Kjellander, D.J. Mitchell, B. Jönsson, *J. Chem. Phys.* **89**, 1664 (1988).

[47] P. Attard, D.J. Mitchell, B.W. Ninham, *J. Chem. Phys.* **88**, 4987 (1988).

[48] R. Podgornik, B. Žekš, *J. Chem. Soc., Faraday Trans. II* **84**, 611 (1988); R. Podgornik, *J. Phys. A: Math. Gen.* **23**, 275

(1990).

[49] J.-L. Barrat, J.-F. Joanny, *Adv. Chem. Phys.* **XCIV**, 1 (1996).

[50] P.A. Pincus, S.A. Safran, *Europhys. Lett.* **42**, 103 (1998).

[51] R. Podgornik, V.A. Parsegian, *Phys. Rev. Lett.* **80**, 1560 (1998).

[52] B.-Y. Ha, A.J. Liu, *Phys. Rev. Lett.* **79**, 1289 (1997); *Phys. Rev. Lett.* **81**, 1011 (1998); *Phys. Rev. E* **58**, 6281 (1998); *Phys. Rev. E* **60**, 803 (1999); *Phys. Rev. Lett.* **83**, 2681 (1999); *Europhys. Lett.* **46**, 624 (1999).

[53] D.B. Lukatsky, S.A. Safran, *Phys. Rev. E* **60**, 5848 (1999).

[54] M. Kardar, R. Golestanian, *Rev. Mod. Phys.* **71**, 1233 (1999).

[55] R.R. Netz, H. Orland, *Eur. Phys. J. E* **1**, 203 (2000).

[56] B.-Y. Ha, *Phys. Rev. E* **64**, 031507 (2001).

[57] A.W.C. Lau, P. Pincus, *Phys. Rev. E* **66**, 041501 (2002).

[58] O. Gonzalez-Amezcua, M. Hernandez-Contreras, P. Pincus, *Phys. Rev. E* **64**, 041603 (2001).

[59] M.J. Stevens, M.O. Robbins, *Europhys. Lett.* **12**, 81 (1990).

[60] A. Diehl, M.N. Tamashiro, M.C. Barbosa, Y. Levin, *Physica A* **274**, 433 (1999); M.C. Barbosa, M. Deserno, C. Holm, *Europhys. Lett.* **52**, 80 (2000).

[61] I. Rouzina, V.A. Bloomfield, *J. Phys. Chem.* **100**, 9977 (1996).

[62] A.A. Kornyshev, S. Leikin, *J. Chem. Phys.* **107**, 3656 (1997); *Phys. Rev. Lett.* **82**, 4138 (1999).

[63] J.J. Arenzon, J.F. Stilck, Y. Levin, *Eur. Phys. J. B* **12**, 79 (1999); Y. Levin, J.J. Arenzon, J.F. Stilck, *Phys. Rev. Lett.* **83**, 2680 (1999).

[64] B.I. Shklovskii, *Phys. Rev. E* **60**, 5802 (1999).

[65] B.I. Shklovskii, *Phys. Rev. Lett.* **82**, 3268 (1999).

[66] A. Yu. Grosberg, T. T. Nguyen, B. I. Shklovskii, *Rev. Mod. Phys.* **74**, 329 (2002).

[67] A. Diehl, H.A. Carmona, Y. Levin, *Phys. Rev. E* **64**, 011804 (2001).

[68] A.W.C. Lau, D. Levine, P. Pincus, *Phys. Rev. Lett.* **84**, 4116 (2000); A.W.C. Lau, P. Pincus, D. Levine, H.A. Fertig, *Phys. Rev. E* **63**, 051604 (2001).

[69] R.R. Netz, *Eur. Phys. J. E* **5**, 557 (2001).

[70] Y. Levin, *Rep. Prog. Phys.* **65**, 1577 (2002).

[71] A. Naji, R.R. Netz, *Eur. Phys. J. E* **13**, 43 (2004).

[72] W.M. Gelbart, R.F. Bruinsma, P.A. Pincus, V.A. Parsegian, *Physics Today* (September 2000), pp. 38-44.

[73] I. Rouzina, V.A. Bloomfield, *Biophys. J.* **74**, 3152 (1998).

[74] R. Golestanian, M. Kardar, T.B. Liverpool, *Phys. Rev. Lett.* **82**, 4456 (1999).

[75] Y. Levin, *Physica A* **265**, 432 (1999).

[76] T.T. Nguyen, I. Rouzina, B.I. Shklovskii, *J. Chem. Phys.* **112**, 2562 (2000).

[77] O. Spalla, L. Belloni, *Phys. Rev. Lett.* **74**, 2515 (1995); L. Belloni, *J. Phys.: Condens. Matter* **12**, R549 (2000).

[78] J. Ray, G.S. Manning, *Macromolecules* **30**, 5739 (1997); *Langmuir* **10**, 2450 (1994).

[79] J.C. Neu, *Phys. Rev. Lett.* **82**, 1072 (1999).

[80] J.E. Sader, D.Y.C. Chan, *J. Colloid Interface Sci.* **213**, 268 (1999); *Langmuir* **16**, 324 (2000).

[81] E. Trizac, J.-L. Raimbault, *Phys. Rev. E* **60**, 6530 (1999); E. Trizac, *Phys. Rev. E* **62**, R1465 (2000).

[82] One can show based on dimensional arguments that the system of counterions at a charged wall has only two independent length scales (*e.g.* the Bjerrum length and the Gouy-Chapman length) and only one independent dimensionless parameter.

[83] M. Baus, J. Hansen, *Phys. Rep.* **59**, 1 (1980).

[84] A more accurate estimate of the typical distance between counterions at low couplings ($\Xi \ll 1$), a , gives $a/\mu \sim \Xi^{1/3}$ taking into account the 3D structure of the counterionic layer.

[85] D. Henderson, L. Blum, *J. Chem. Phys.* **75**, 2025 (1981); S.L. Carnie, D.Y.C. Chan, *J. Chem. Phys.* **74**, 1293 (1981); H. Wenneström, B. Jönsson, P. Linse, *J. Chem. Phys.* **76**, 4665 (1982).

[86] Y. Burak, D. Andelman, H. Orland, *Phys. Rev. E* **70**, 016102 (2004).

[87] A.G. Moreira, *Charged systems in bulk and at interfaces*, Ph.D. dissertation, Potsdam University (2001).

[88] S. Jungblut, R.R. Netz, unpublished; S. Jungblut, Diploma dissertation, Ludwig Maximilian University Munich (2004).

[89] G.S. Manning, *J. Chem. Phys.* **51**, 924 (1969).

[90] B.H. Zimm, M. Le Bret, *J. Biomol. Struct. Dyn.* **1**, 461 (1983); M. Le Bret, B.H. Zimm, *Biopolymers* **23**, 287 (1984).

[91] A. Naji, R.R. Netz, submitted to *Phys. Rev. Lett.* (2005).

[92] Note that γ_{RB} may be related to the coupling parameter as $\gamma_{RB} = \Xi/(\xi\tilde{\Delta})$, where $\tilde{\Delta} = \Delta/\mu$.

[93] A. Diehl, M.C. Barbosa, Y. Levin, *Europhys. Lett.* **53**, 86 (2001).

[94] A.G. Moreira, R.R. Netz, *Europhys. Lett.* **57**, 911 (2002).